Med

Theranostic methodology for *ex vivo* donor lung rehabilitation

Graphical abstract

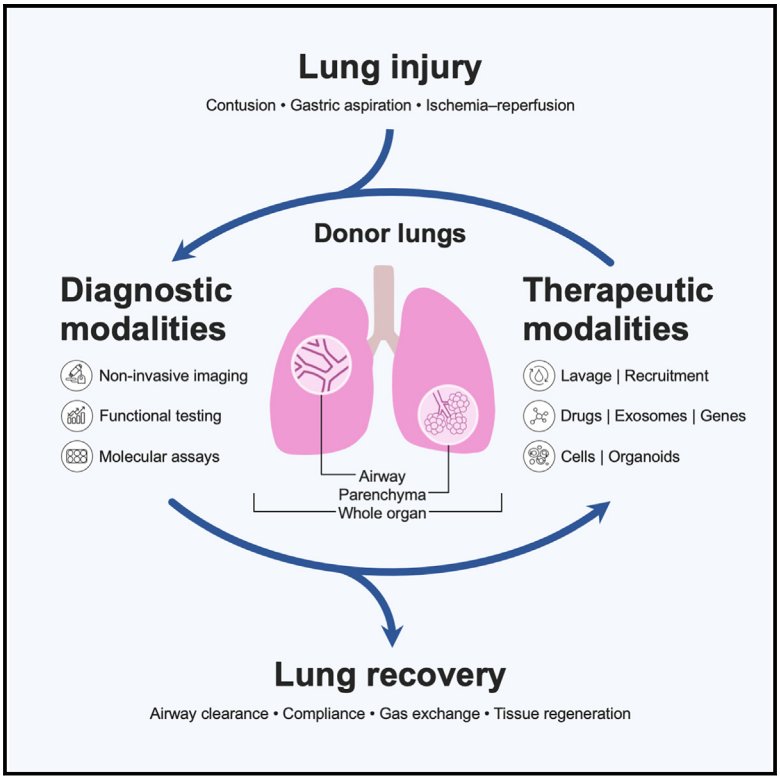

Highlights

- Donor lungs with various types of injuries were recovered using cross-circulation
- Diagnostic modalities enabled assessment of airway and parenchymal health in lungs
- Cells and organoids were delivered and tracked using advanced imaging techniques

Authors

Meghan R. Pinezich, John D. O'Neill, Brandon A. Guenthart, ..., Hans-Willem Snoeck, Matthew Bacchetta, Gordana Vunjak-Novakovic

Correspondence

gv2131@columbia.edu

In brief

Cross-circulation with swine can support injured donor lungs for several days; however, robust diagnostic modalities and therapeutic interventions are needed. Pinezich et al. report a therapeutic and diagnostic ("theranostic") methodology for evaluation and functional recovery of injured donor lungs during cross-circulation.

Pre-clinical Research

Pinezich et al., 2025, Med *6*, 100644
July 11, 2025
https://doi.org/10.1016/j.medj.2025.100644

CellPress

Please cite this article in press as: Pinezich et al., Theranostic methodology for *ex vivo* donor lung rehabilitation, Med (2025), https://doi.org/10.1016/j.medj.2025.100644

Med

CellPress

Resource

Theranostic methodology for *ex vivo* donor lung rehabilitation

Meghan R. Pinezich,[1] John D. O'Neill,[1] Brandon A. Guenthart,[2] Jinho Kim,[3] Olaia F. Vila,[1] Stephen P. Ma,[1] Ya-Wen Chen,[4] Ahmed E. Hozain,[1,5] Aravind Krishnan,[2] Moeed Fawad,[2] Katherine M. Cunningham,[1] Holly M. Wobma,[1] Julie Van Hassel,[1,5] Hans-Willem Snoeck,[4,6,7] Matthew Bacchetta,[8] and Gordana Vunjak-Novakovic[1,4,9,*]

[1]Department of Biomedical Engineering, Columbia University, New York, NY, USA
[2]Department of Cardiothoracic Surgery, Stanford University, Stanford, CA, USA
[3]Department of Biomedical Engineering, Stevens Institute of Technology, Hoboken, NJ, USA
[4]Department of Medicine, Columbia University Irving Medical Center, New York, NY, USA
[5]Department of Surgery, Columbia University Irving Medical Center, New York, NY, USA
[6]Department of Microbiology and Immunology, Columbia University Irving Medical Center, New York, NY USA
[7]Columbia Center for Human Development, Columbia University Irving Medical Center, New York, NY, USA
[8]Departments of Cardiac Surgery and Biomedical Engineering, Vanderbilt University, Nashville, TN, USA
[9]Lead contact
*Correspondence: gv2131@columbia.edu
https://doi.org/10.1016/j.medj.2025.100644

CONTEXT AND SIGNIFICANCE The supply of donor lungs for transplantation is not sufficient to meet demand, and many patients die waiting for an organ. Currently, about 80% of donor lungs are not acceptable for transplant, often due to injury. Cross-circulation is an advanced *ex vivo* lung perfusion technique used to keep injured donor organs alive outside of the body and restore them to a quality that is acceptable for transplantation. This resource reports a methodology for therapeutic and diagnostic ("theranostic") intervention to rehabilitate donor lungs during cross-circulation. Application of the theranostic methodology during cross-circulation could enable the salvage of donor lungs and thereby increase the number of lungs available for transplant and reduce waitlist mortality.

SUMMARY

Background: About 80% of donor lungs are not utilized for transplantation. Cross-circulation of *ex vivo* lungs with a support swine enables the rehabilitation of donor lungs that are initially deemed unsuitable for transplantation. Robust therapeutic and diagnostic modalities are needed for *ex vivo* lung rehabilitation; however, no standardized "theranostic" methodology has been reported.

Methods: *Ex vivo* lungs (n = 23; 17 injured and 6 controls) with multi-focal contusion (n = 6, human), gastric aspiration injury (n = 8, swine), ischemia-reperfusion injury (n = 3, swine), or no injury (n = 6, swine) were used to develop a therapeutic and diagnostic (theranostic) methodology for *ex vivo* lung rehabilitation during cross-circulation. Airway (bronchoscopic, nebulized), intravascular, and transpleural access enabled sample collection and therapeutic delivery. Diagnostic modalities included non-invasive imaging, functional testing, and molecular assays. Therapeutic modalities included bronchoalveolar lavage, surfactant replacement, recruitment maneuvers, and cell/organoid delivery. Real-time tracking of delivered cells was performed via fluorescence and bioluminescence imaging.

Findings: Diagnostic assessments revealed tissue-, cell-, and molecular-level insights at global and regional scales of *ex vivo* lungs during cross-circulation, which informed therapeutic management and interventions to recover donor lungs. Mesenchymal stromal cells and lung organoids were delivered bronchoscopically and transpleurally, tracked non-invasively during cross-circulation, and observed to localize within the parenchyma.

Conclusions: Application of a theranostic methodology during cross-circulation enabled real-time *ex vivo* lung assessment and rehabilitation across a variety of lung injuries to help increase clinical utilization of donor lungs in the future.

Funding: NIH (P41 EB027062, R01HL120046, U01HL134760), CFF (VUNJAK23XX0).

Please cite this article in press as: Pinezich et al., Theranostic methodology for *ex vivo* donor lung rehabilitation, Med (2025), https://doi.org/10.1016/j.medj.2025.100644

INTRODUCTION

Donor lungs are largely underutilized; about 80% are declined for transplantation, often due to functional impairment or acute injury.[1,2] Most prevalent donor lung injuries, including contusion, gastric aspiration, and ischemia-reperfusion injury, are potentially reversible *ex vivo*, but repair requires systemic physiologic support and sufficient rehabilitation time to enable therapeutic intervention. Isolated *ex vivo* lung perfusion (EVLP), indicated for *ex vivo* preservation of donor lungs meeting standard criteria for transplant and for re-assessment of marginal quality donor lungs, has facilitated transplantation of over 1,000 lungs in the past 20 years.[3,4] However, clinical EVLP remains limited to 4–6 h of support, precluding recovery of severely injured lungs.

Our group was the first to develop a cross-circulation platform for *ex vivo* lung rehabilitation.[3,5–8] During cross-circulation blood is continuously exchanged between the organ and a support swine acting as an integrated systemic physiologic bioreactor to provide a homeostatic recovery environment. Using a standard immunosuppression regimen informed by established protocols and current practices in clinical lung transplantation,[9] we showed that cross-circulation can restore injured donor lungs to transplant quality[5,7] and support *ex vivo* lungs for over 4 days.[6] Thus, cross-circulation offers the physiological support and time needed for the rehabilitation of *ex vivo* lungs.

To facilitate clinical translation of cross-circulation, standardized diagnostic and therapeutic modalities are needed. While diagnostic assessments during clinical EVLP typically evaluate basic functional parameters (e.g., airway pressure, PaO_2/FiO_2, pulmonary vascular resistance), cross-circulation offers the time and opportunity for comprehensive longitudinal evaluation of tissue, cell, and molecular properties to inform therapeutic intervention, monitor improvement, and determine transplant suitability. Diagnostic modalities should (1) assess clinically relevant global and/or local lung functions, (2) enable evaluation of airway, parenchymal, and vascular health, (3) utilize non-destructive methods, and (4) provide real-time feedback for longitudinal analyses and personalized intervention. For the highest impact, therapeutic approaches should leverage both standard clinical methods (e.g., bronchoalveolar lavage [BAL], recruitment maneuvers) and emerging therapeutic interventions (e.g., cell/gene therapy) to rehabilitate donor lungs with severe injuries.

Informed by our group's 10 years of experience developing cross-circulation, we describe our ''theranostic'' (i.e., therapeutic and diagnostic) methodology for donor lung rehabilitation, including integrated non-invasive imaging, functional testing, molecular assays, and real-time tracking of delivered cells (Figure 1A). We use the term theranostic to describe not only modalities that have both therapeutic and diagnostic applications (e.g., bronchoscopy) but also the overarching methodology that integrates application of therapeutic and diagnostic modalities for *ex vivo* lung rehabilitation (Figure S1). We developed and validated this comprehensive methodology for implementation in two settings: cross-circulation and isolated EVLP of lungs with a variety of injuries that preclude their use for transplantation (Figure 1B). We envision that this theranostic methodology will help establish a foundation for bench-to-bedside translation of cross-circulation as a platform for *ex vivo* rehabilitation of injured donor lungs for transplantation.

RESULTS

Diagnostic and therapeutic modalities were developed during cross-circulation and isolated EVLP of lungs with gastric aspiration (primary insult to respiratory epithelium), ischemia-reperfusion injury (primary insult to respiratory endothelium), and multi-focal contusion (impact on ventilation/perfusion [V/Q] ratio) (Figures 2 and S2). Multiple access strategies, including airway (bronchoscopic, nebulized), intravascular, and transpleural approaches, were used for *ex vivo* lung rehabilitation in these settings (Figure S3). We report representative results for each modality by longitudinal comparison between two time points (e.g., baseline versus endpoint) and additional assessments at a single time point (e.g., midpoint, endpoint), as applicable in clinical decision-making during *ex vivo* lung evaluation.

Whole-organ and regional tissue perfusion diagnostic modalities for *ex vivo* lungs

Surface temperature imaging

Thermography enables real-time, non-invasive, high-sensitivity evaluation of lung surfaces, and has been used to identify lungs with poor function after EVLP support.[10] We conducted standardized lung surface temperature imaging using a thermal camera at the start of lung reperfusion to identify poorly perfused regions and inform corrective action (e.g., pulmonary artery [PA] cannula repositioning) and to periodically assess injured regions and inform therapeutic intervention (e.g., recruitment maneuvers) during cross-circulation (Figure S4A).[5,7,8] In lungs with localized injury (e.g., contusion, gastric aspiration), increased surface temperature correlated with injured regions (Figures 3A and S5A), while decreased surface temperature correlated with improvements in function (increased PaO_2/FiO_2 and compliance) and histomorphology (reduced edema and interstitial infiltrates) (Figure S5B). Surface temperature imaging enabled clinically relevant whole-organ and regional tissue assessment of reperfusion and injury and can thus guide therapeutic intervention during cross-circulation and isolated EVLP.

Lung weight

Lung weight, a marker of pulmonary edema that can be measured non-destructively, has been correlated with transplant suitability and clinical outcomes, including primary graft dysfunction, length of hospital stay, and mortality.[11,12] In the present study, lung weight was measured at baseline (i.e., immediately after explant) and throughout cross-circulation.[5,7,8] Lung weight gain was often observed after reperfusion due to increased vascular permeability. In swine lungs with gastric aspiration injury, weight gain of up to 20% above baseline occurred within the first 12 h, and return to baseline lung weight often required more than 12 h of *ex vivo* rehabilitation (Figure 3B).

Visualization of global perfusion

Direct radiographic assessment without chest wall interference is a distinct advantage of EVLP. Blinded radiographic scoring

Please cite this article in press as: Pinezich et al., Theranostic methodology for *ex vivo* donor lung rehabilitation, Med (2025), https://doi.org/10.1016/j.medj.2025.100644

CellPress

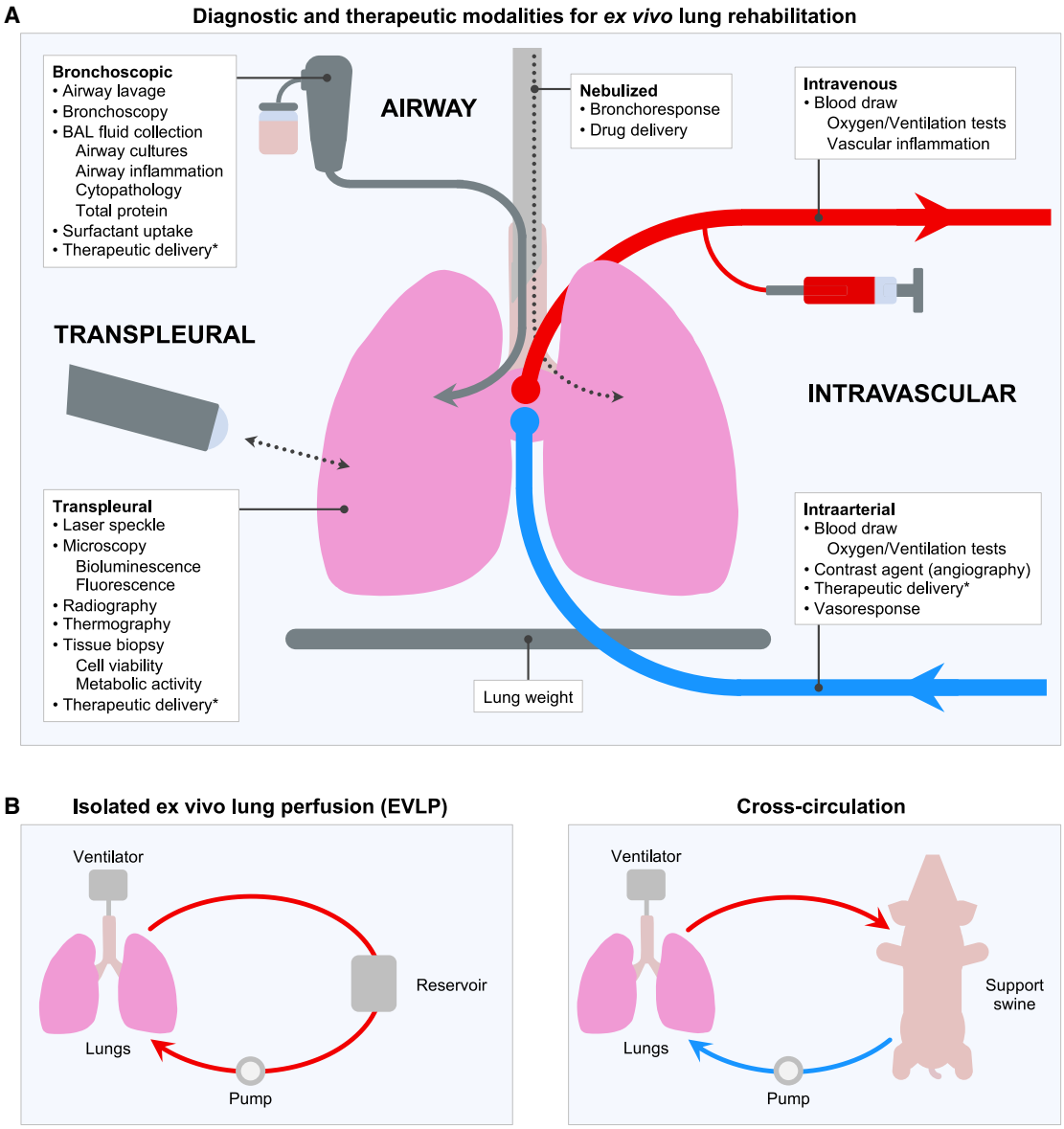

Figure 1. Diagnostic and therapeutic modalities for *ex vivo* lung rehabilitation

(A) Access strategies to perform diagnostic assessments and therapeutic interventions in *ex vivo* lungs include airway (bronchoscopic, nebulized), intravascular, and transpleural approaches. *Therapeutic delivery may include cells, drugs, exosomes, genes, organoids, RNA transcripts, surfactant, and/or other agents. (B) Strategies to support *ex vivo* lungs. BAL, bronchoalveolar lavage.

during EVLP was previously shown to predict transplant suitability.[13] In this study, radiography was performed (1) to confirm cannula and/or bronchoscope placement; (2) to assess atelectasis, consolidation, and infiltration; and (3) to assess pulmonary vascular integrity.[7] Specifically, contrast angiography was performed via intravascular delivery of a contrast agent to assess patency and perfusion of the pulmonary vasculature, which is often compromised in injured lungs (Figure S4A). Radiography of injured lungs at baseline revealed consolidation, infiltration, and vascular leakage consistent with alveolar-capillary barrier disruption. Radiography, including angiography at endpoint, was used to confirm patency and perfusion of the pulmonary vasculature and aeration within the parenchyma (resolution of consolidation) (Figure 3C).

Visualization of regional perfusion

Regional perfusion differences in *ex vivo* lungs may be due to edema, pulmonary hypertension, thrombi, vasoconstriction, and other causes. In all cases, regional perfusion analysis can identify vascular abnormalities. In particular, vascular thrombi are found in up to 35% of donor lungs and are difficult to detect using standard diagnostic modalities, presenting significant risk to post-operative outcomes.[14] Laser speckle

Please cite this article in press as: Pinezich et al., Theranostic methodology for *ex vivo* donor lung rehabilitation, Med (2025), https://doi.org/10.1016/j.medj.2025.100644

A

Lung injury	Species	Mode of injury	Endpoint*	Reference
Multi-focal contusion	Human	Bilateral thoracic trauma before donation	24 hours	Hozain 2020
Gastric aspiration	Swine	Airway delivery of gastric contents (6 h dwell) before explant	36 hours	Guenthart 2019
Ischemia–reperfusion	Swine	Cold ischemia (4°C, 18 h) after explant	36 hours	O'Neill 2017
Control	Swine	None	36 hours	O'Neill 2017
			120 hours	Hozain 2019

* Duration of cross-circulation between *ex vivo* lungs and a support swine from Baseline to Endpoint

B

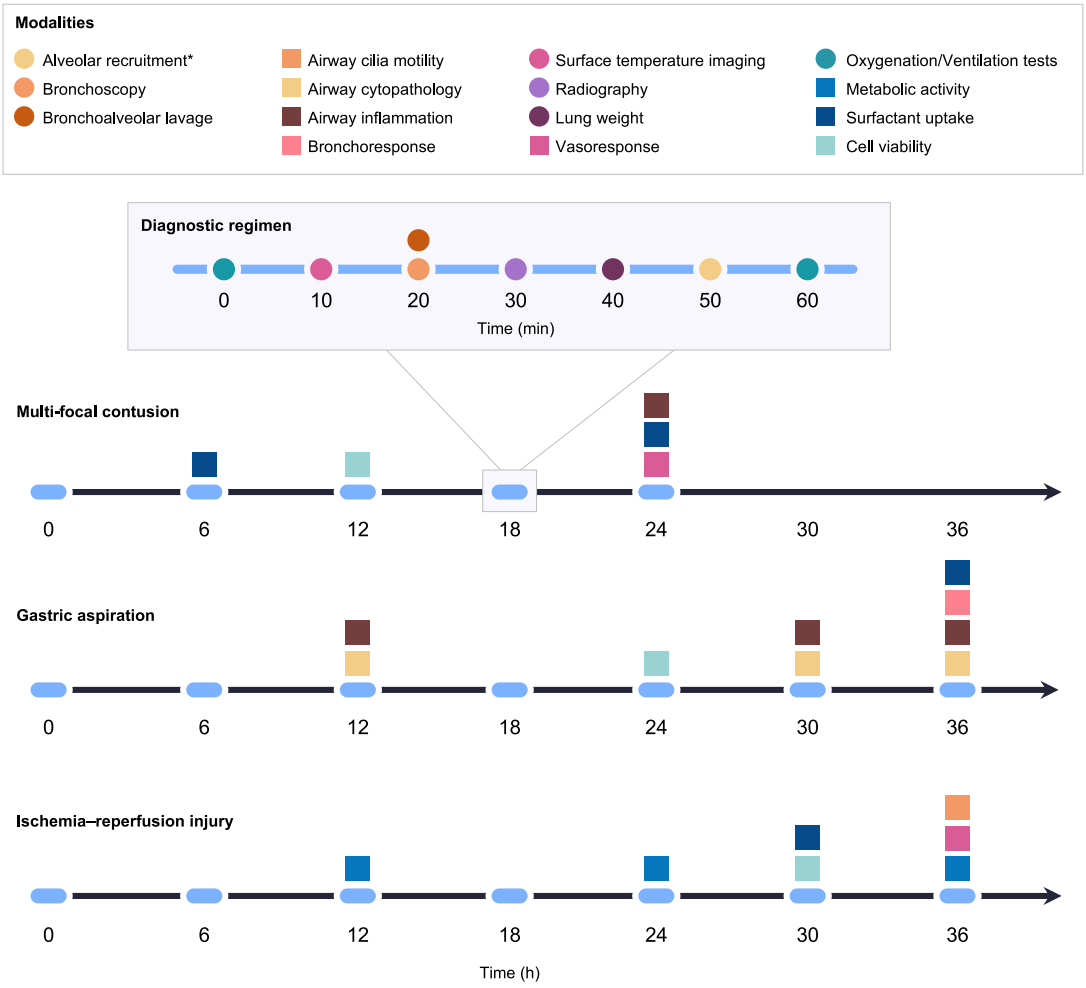

Figure 2. Exemplary theranostic regimens for *ex vivo* lung rehabilitation

(A) Exemplary injuries of *ex vivo* lungs used to develop diagnostic and therapeutic modalities.

(B) Theranostic regimens developed for rehabilitation of *ex vivo* lungs with multi-focal contusion, gastric aspiration, and ischemia-reperfusion injury. Other permutations of diagnostic and/or therapeutic modalities may be required depending on type and severity of lung injury. *Alveolar recruitment: manual and/or ventilator maneuvers, with surfactant replacement (bronchoscopic delivery of surfactant) as needed.

contrast imaging (LSCI) offers real-time, non-invasive, quantitative insights into the perfusion and recovery trajectory of injured lung regions. In this study, an LSCI system configured for *ex vivo* lung evaluation revealed quantitative differences in regional perfusion (Figure S4A). Perfusion of injured, atelectatic lung regions (145 ± 19 U/cm^2) was significantly lower than in normal, well-ventilated lung regions (332 ± 119 U/cm^2) (Figure 3D).

Airway tissue, cell, and molecular diagnostic modalities for *ex vivo* lungs

Bronchoscopy

Bronchoscopy is versatile and minimally invasive, thus offering significant theranostic value. In the present study, bronchoscopy was used to perform BAL, visualize airways, and collect BAL fluid for downstream cellular and molecular diagnostics.[5,7,8] In lungs with severe injury, BAL was performed to

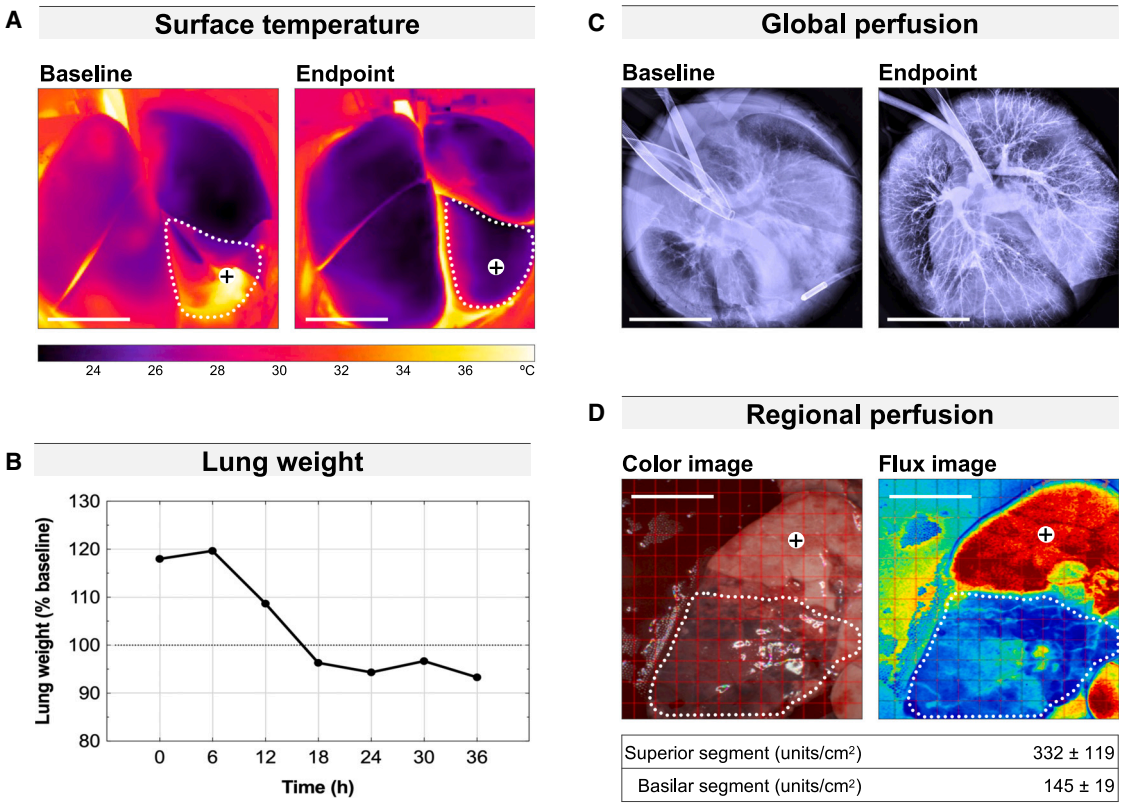

Figure 3. Whole-organ and regional tissue perfusion diagnostic modalities for *ex vivo* lungs, representative case assessments

(A) Surface temperature imaging of human donor lungs with multi-focal contusion using an infrared camera during cross-circulation. Dotted line indicates region with contusion. Scale bar: 10 cm.

(B) Lung weight of swine lungs with gastric aspiration using a digital scale during cross-circulation. Baseline indicates lung weight immediately after explant.

(C) Global perfusion imaging with contrast angiography of human donor lungs with multi-focal contusion using an X-ray unit during cross-circulation. Scale bar: 10 cm.

(D) Regional perfusion imaging of human donor lungs with multi-focal contusion using a laser speckle contrast imaging system during isolated *ex vivo* lung perfusion (EVLP). Dotted line indicates region of lower lobe with significant consolidation. Scale bar: 5 cm.

remove excess fluid and cellular debris, and therapeutic surfactant was administered by bronchoscopic delivery. In lungs with gastric aspiration injury, bronchoscopy at baseline showed airway inflammation, erythema, and secretions. After 36 h of cross-circulation, airways appeared clear with minimal inflammation and no erythema (Figure 4A).

Bronchoresponse

Methacholine challenge, a sensitive bronchoprovocation test used to diagnose asthma, measures airway pressure in response to nebulized methacholine. In the present study, methacholine challenge was performed to evaluate smooth muscle viability and tone in *ex vivo* lungs.[7] After 24 h of cross-circulation, human donor lungs with multi-focal contusion showed an approximately 100% increase in peak inspiratory pressure in response to nebulized methacholine, confirming airway smooth muscle tone, an important function in lung grafts (Figure 4B). In lung transplant recipients, a positive methacholine challenge result (i.e., <8 mg/mL methacholine required to reduce forced expiratory volume in 1 s by 20%) at 3 months after transplant correlated with the likelihood of developing chronic lung allograft dysfunction (CLAD).[16] Future studies are needed to investigate the prognostic implications of methacholine challenge during *ex vivo* lung rehabilitation and to determine how responses to bronchoprovocation challenges during *ex vivo* support correlate with transplant outcomes.

Airway cilia motility

Mucociliary clearance is a crucial airway function that requires coordinated movement of airway cilia and can be compromised in transplant recipients for up to 12 weeks post-transplant.[17] In the present study, airway cilia motility was assessed at endpoint using high-speed fluorescence imaging to monitor the movement of fluorescent microparticles delivered to the luminal surface of the airway (Figure 4C). In lungs with severe ischemia-reperfusion injury, the airway epithelium is also susceptible to cellular disruption and apoptosis. However, coordinated cilia beating driving the directional flow of microparticles was observed at endpoint (Data S1). While traditionally performed on dissected airway samples using an inverted fluorescence microscope, the airway cilia motility test can also be conducted *in situ* using a fluorescence broncho-microscope (Figure S4B; Data S1).

Please cite this article in press as: Pinezich et al., Theranostic methodology for *ex vivo* donor lung rehabilitation, Med (2025), https://doi.org/10.1016/j.medj.2025.100644

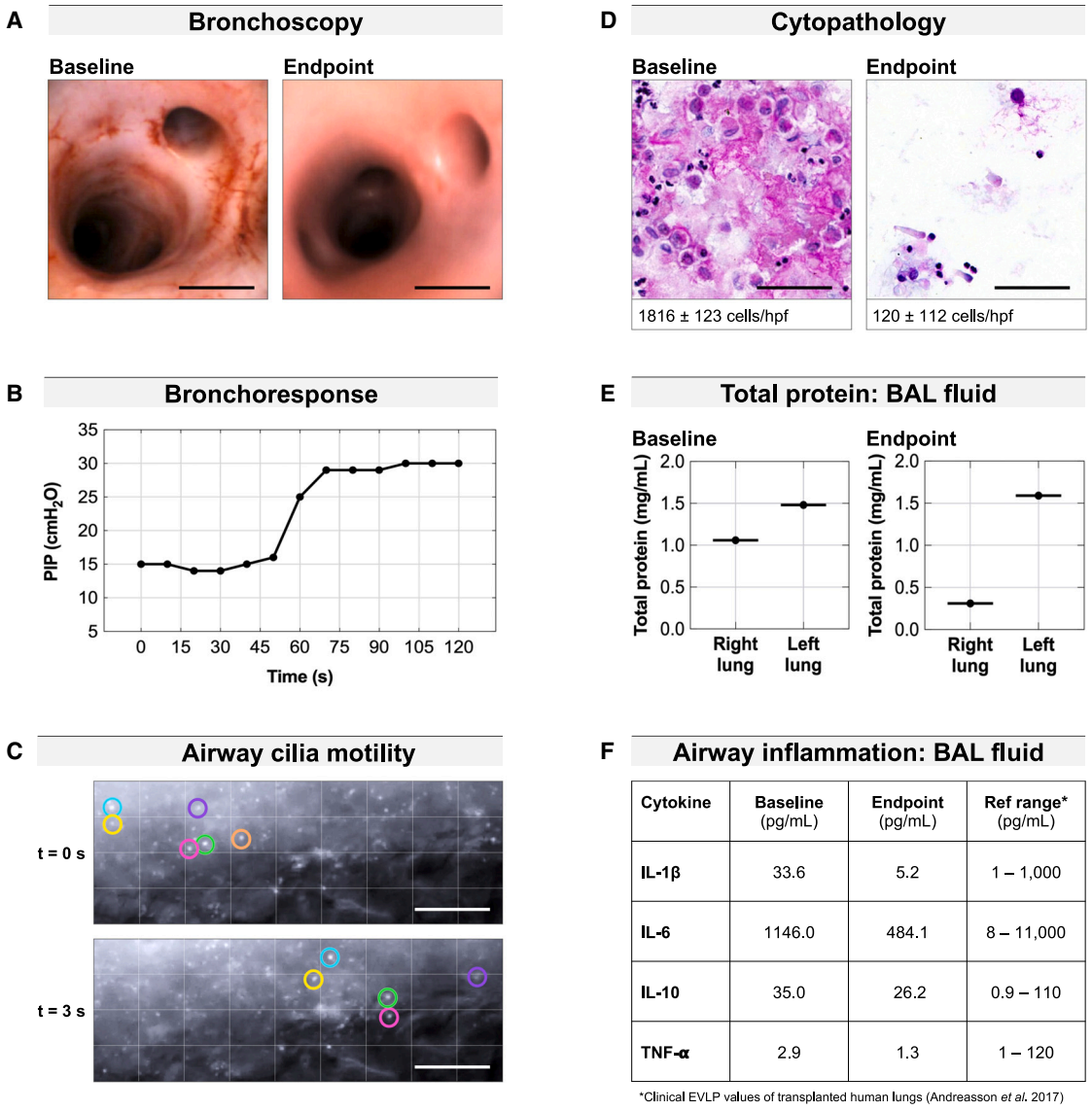

Cytokine	Baseline (pg/mL)	Endpoint (pg/mL)	Ref range* (pg/mL)
IL-1β	33.6	5.2	1 – 1,000
IL-6	1146.0	484.1	8 – 11,000
IL-10	35.0	26.2	0.9 – 110
TNF-α	2.9	1.3	1 – 120

*Clinical EVLP values of transplanted human lungs (Andreasson *et al.* 2017)

Figure 4. Airway tissue, cell, and molecular diagnostic modalities for *ex vivo* lungs, representative case assessments

(A) Bronchoscopy of swine lungs with gastric aspiration using a video bronchoscope during cross-circulation. Scale bar: 10 mm.

(B) Bronchoresponse of human donor lungs with multi-focal contusion using nebulized administration of methacholine (bronchoconstrictor) during cross-circulation. PIP, peak inspiratory pressure.

(C) Airway cilia motility assessment in swine lungs with ischemia-reperfusion injury using a fluorescence microscope and high-speed camera during cross-circulation. Scale bar: 10 μm.

(D) Cytopathology of BAL fluid smears of swine lungs with gastric aspiration using periodic acid-Schiff staining and a bright-field microscope during cross-circulation. Scale bar: 100 μm. hpf, high-power field.

(E) Total protein in BAL fluid of human donor lungs with bilateral multi-focal contusion using Coomassie Bradford protein assay during cross-circulation.

(F) Airway inflammatory cytokines in BAL fluid of human lungs with multi-focal contusion using enzyme-linked immunosorbent assays during cross-circulation. Reference range specifies values reported for clinical EVLP of transplanted human lungs.[15]

BAL fluid

Total protein and inflammatory cytokine concentrations in BAL fluid serve as key indicators of lung injury severity and immune response, facilitating assessment of transplant suitability. Concentrations of interleukin-6 (IL-6) and IL-8 in BAL fluid after transplant correlated with increased length of hospital stay and higher risk of CLAD.[18] Gross appearance of BAL fluid at baseline and endpoint correlated with quantitative data for cell numbers (Figures 4D and S6A) and total protein (by Bradford assay, Figure S6B). Previous studies in *ex vivo* swine lungs showed that BAL fluid from lungs with gastric aspiration injury had a total protein concentration $\gtrsim$1.5 mg/mL, while control lungs had a total protein concentration $\lesssim$0.8 mg/mL.[5,8] The elevated total protein concentration in BAL fluid corresponded

Please cite this article in press as: Pinezich et al., Theranostic methodology for *ex vivo* donor lung rehabilitation, Med (2025), https://doi.org/10.1016/j.medj.2025.100644

to regional injury and indicated increased permeability of the alveolar-capillary barrier. In human lungs with bilateral multi-focal contusion, total protein from baseline to endpoint decreased in the right lung but remained relatively constant in the left lung (Figure 4E), suggesting different levels of recovery in the right and left lungs.[5] In human lungs with multi-focal contusion, IL-1β, IL-6, and tumor necrosis factor-α concentrations decreased by 84.5%, 57.7%, and 55.2%, respectively, from baseline to endpoint, while IL-10 concentrations were maintained (Figure 4F).[7,15]

Parenchymal cell and tissue diagnostic modalities for *ex vivo* lungs

Oxygenation test

Proper ventilator management has been shown to mitigate risk of primary graft dysfunction. Protective ventilation during EVLP reduced lung inflammation and length of hospital stay in lung transplant recipients.[19–21] In the present study, PaO_2/FiO_2 measurements were performed throughout cross-circulation to assess gas exchange capacity and oxygenation of lungs in response to alterations in ventilation parameters (challenge). Minute ventilation was increased by 100%, and FiO_2 was increased to 100% for 5 min, followed by blood sample collection for blood gas analysis.[5,7,8] In lungs with gastric aspiration injury, increased minute ventilation and FiO_2 resulted in only minor increases in PaO_2 at the initiation of cross-circulation. However, after 36 h of *ex vivo* lung rehabilitation, increased levels of inhaled oxygen resulted in significant increases in PaO_2. The difference in pre- and post-challenge oxygenation increased from +18 cmH_2O at baseline to +318 cmH_2O at endpoint (Figure 5A).

Ventilation test

Monitoring carbon dioxide unloading in *ex vivo* lungs can provide decisive insights into lung function beyond oxygenation measurements alone.[22] In the present study, carbon dioxide unloading from blood was assessed by measuring pCO_2 before and after the change in ventilation parameters (challenge). Minute ventilation was increased by 100%, and FiO_2 was increased to 100% for 5 min, as for the oxygenation test.[5,7,8] In donor lungs with multi-focal contusion, baseline post-challenge pCO_2 was lower than pre-challenge pCO_2, indicating extremely poor ventilation. However, at endpoint, the difference between pre- and post-challenge pCO_2 increased by 19 cmH_2O to +10 cmH_2O, indicating significantly improved ventilation. Depending on injury type, oxygenation or ventilation testing may be more informative for *ex vivo* lung management and rehabilitation (Figure 5B).

Vasoresponse

The pulmonary vasculature constricts in response to alveolar hypoxia to optimize systemic oxygen delivery and compensate for V/Q mismatch. Hypoxic pulmonary vasoconstriction challenges have been suggested as metrics for donor lung evaluation during EVLP, in which decreased hypoxic vasoconstriction correlated with lung inflammation.[23] In the present study, pulmonary vasoconstriction was evaluated at endpoint by intravascular administration of epinephrine.[5,7,8] Pulmonary artery pressure typically increased by 10–12 mmHg in all lung injuries evaluated, confirming vasoresponse in *ex vivo* lungs (Figure 5C).

Metabolic activity

In lung transplant patients, metabolic activity measurements can differentiate restrictive allograft syndrome from bronchiolitis obliterans.[24] Given the importance of metabolic activity in lung health, real-time metabolic activity was assessed throughout cross-circulation using alamarBlue Cell Viability Reagent to monitor parenchymal metabolism in *ex vivo* lungs.[5,7,8] In lungs with ischemia-reperfusion injury, metabolic activity increased nearly 10-fold throughout cross-circulation, indicating significant recovery of parenchymal metabolism (Figure 5D). Over the course of *ex vivo* lung rehabilitation, metabolic activity increased from baseline to endpoint and typically returned to levels close to those in control lungs,[6] suggesting recovery of cellular metabolism during cross-circulation.

Cell viability

Acute lung injury, including ischemia-reperfusion injury, is a major contributor to oxidative stress and cell death. Airway and parenchymal cell viability in *ex vivo* lungs are essential to ensure graft health after transplantation, as injury and ischemic cell death following reperfusion accelerates inflammation in the recipient.[25] Cell viability was confirmed in different regions of *ex vivo* lungs by visualizing the uptake of fluorescent cell viability marker carboxyfluorescein succinimidyl ester (CFSE).[5,7,8] Pervasive uptake of CFSE in human lungs with multi-focal contusion confirmed the viability of parenchymal cells at endpoint (Figure 5E).

Surfactant uptake

Surfactant delivery to *ex vivo* lungs has theranostic value because it can serve as an indicator of type II pneumocyte function (diagnostic) and can improve atelectasis (therapeutic).[5,26] Surfactant gene and protein expression in type II pneumocytes has been correlated with transplant outcomes, including correlation of poor type II cell function with primary graft dysfunction.[27,28] In this study, type II pneumocytes in human lungs with multi-focal contusion were assessed by visualization of the uptake of fluorescent-tagged surfactant protein B (SPB) (Figure 5F), confirming the viability and function of type II cells and indicating parenchymal recovery.[7] Due to the relatively small delivery volumes, surfactant uptake was only used to evaluate regions where type II cell function and parenchymal recovery were of critical interest for assessment and treatment of localized lung injury.

Real-time tracking of putative therapeutics in *ex vivo* lungs

Fluorescence tracking

To enable real-time, non-destructive tracking of cell-based deliverables, we developed a transpleural fluorescence imaging system (Figures 6A and 6B). Mesenchymal stromal cells (MSCs) and lung organoids were tracked after delivery into control *ex vivo* lungs using real-time automated fluorescence and post-treatment analysis (Figure 6C; Data S1). MSCs are a putative cell therapy due to their immunomodulatory potential, based on a range of pre-clinical and clinical studies of EVLP support.[29–31] MSCs labeled with CFSE or CellBrite were delivered in liquid micro-volume plugs using a microcatheter delivery system under bronchoscopic guidance (Figure S7A) and visualized using a transpleural fluorescence imaging system under continuous ventilation during cross-circulation. A custom cell-tracking algorithm utilizing

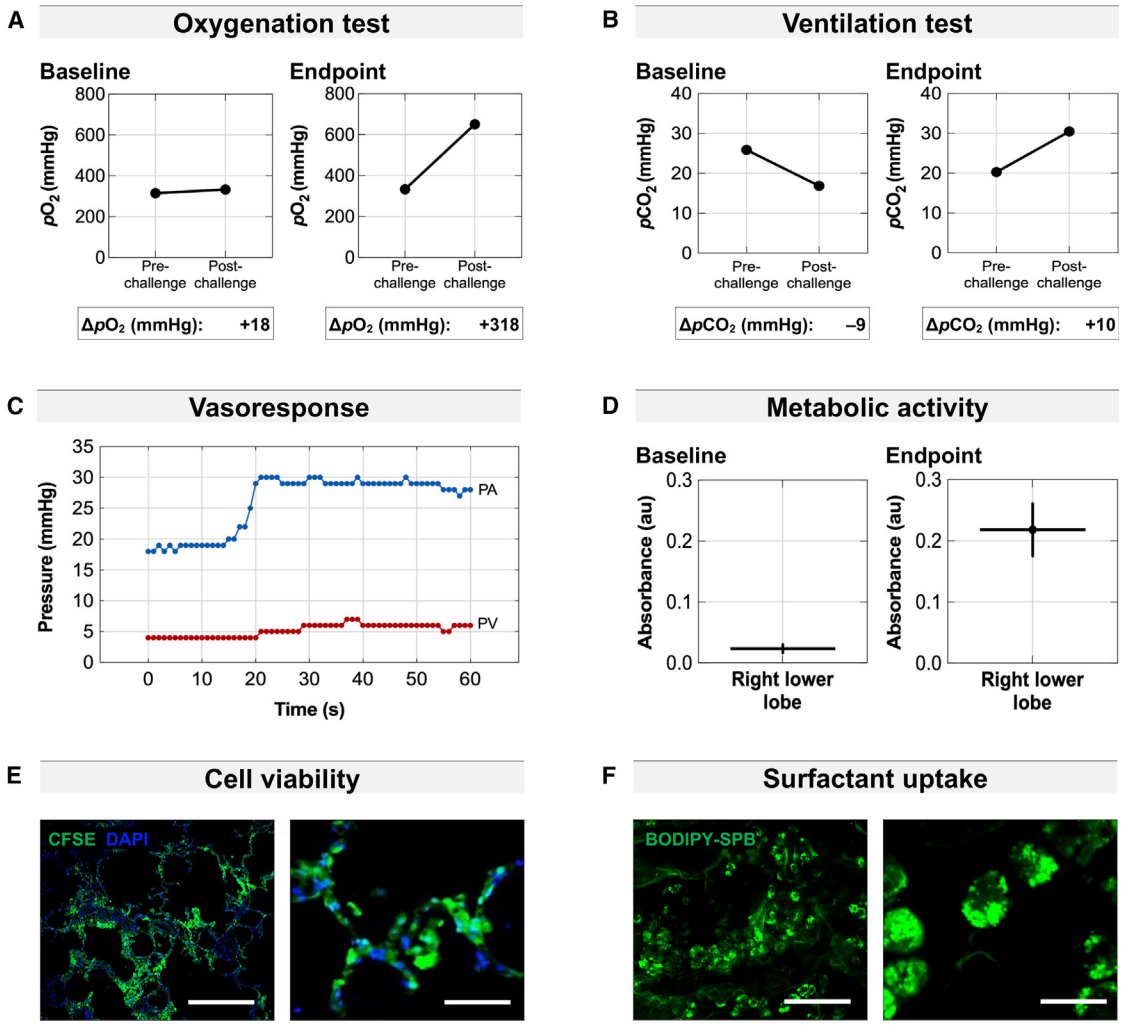

Figure 5. Parenchymal cell and tissue diagnostic modalities for *ex vivo* lungs, representative case assessments

(A) Oxygenation test of swine lungs with gastric aspiration using blood gas analyzer during cross-circulation. $pO_2 = \Delta|(PA - PV)|$, where PA = pO_2 at pulmonary artery, and PV = pO_2 at pulmonary vein. $\Delta pO_2 = \Delta$(post-challenge – pre-challenge), where post-challenge = $\Delta(pO_2)$ after challenge, and pre-challenge = $\Delta(pO_2)$ before challenge.

(B) Ventilation test of swine lungs with gastric aspiration using blood gas analyzer during cross-circulation. $pCO_2 = \Delta|(PA - PV)|$, where PA = pCO_2 at pulmonary artery and PV = pCO_2 at pulmonary vein. $\Delta pCO_2 = \Delta$(post-challenge – pre-challenge), where post-challenge = $\Delta(pCO_2)$ after challenge and pre-challenge = $\Delta(pCO_2)$ before challenge. PA, pulmonary artery; PV, pulmonary vein.

(C) Vasoresponse of human donor lungs with multi-focal contusion using intravascular administration of epinephrine (vasoconstrictor) during isolated EVLP. PA, blue; PV, red.

(D) Metabolic activity (mean ± standard deviation of technical replicates) of swine lungs with ischemia-reperfusion injury using resazurin-based assay during cross-circulation. au, arbitrary unit.

(E) Cell viability of human donor lungs with multi-focal contusion using transpleural administration of carboxyfluorescein diacetate succinimidyl ester (CFSE) and fluorescence microscope during cross-circulation. Scale bars: 250 μm (left), 50 μm (right).

(F) Surfactant uptake of human donor lungs with multi-focal contusion using transpleural administration of surfactant protein B tagged with green fluorescent dye (BODIPY-SPB) and fluorescence microscope during cross-circulation. Scale bars: 100 μm (left), 20 μm (right).

computer vision integrated with machine learning was applied to identify and quantify the delivered cells in real time (Figure 6C; Data S1). Real-time transpleural fluorescence imaging was performed in distal lung regions due to the limited penetrative depth of fluorescent light through lung parenchymal tissue.

As a potential alternative to cell therapy, MSC-derived exosomes were also isolated from *in vitro* MSC culture and delivered as a putative cell-derived therapeutic during cross-circulation (Figure S7B). Organoids also represent interesting cell therapy candidates because they contain multi-potent lung progenitor cells that give rise to proximal airway-like and alveolar-like structures *in vitro*.[32] Delivery of lung-specific cell types could enable selective replacement of damaged lung cells or localized release of reparative lung-specific signals. Lung organoids were delivered via bronchoscopy or transpleural injection (Data S1) into distal regions of *ex vivo* swine lungs (controls with no injury)

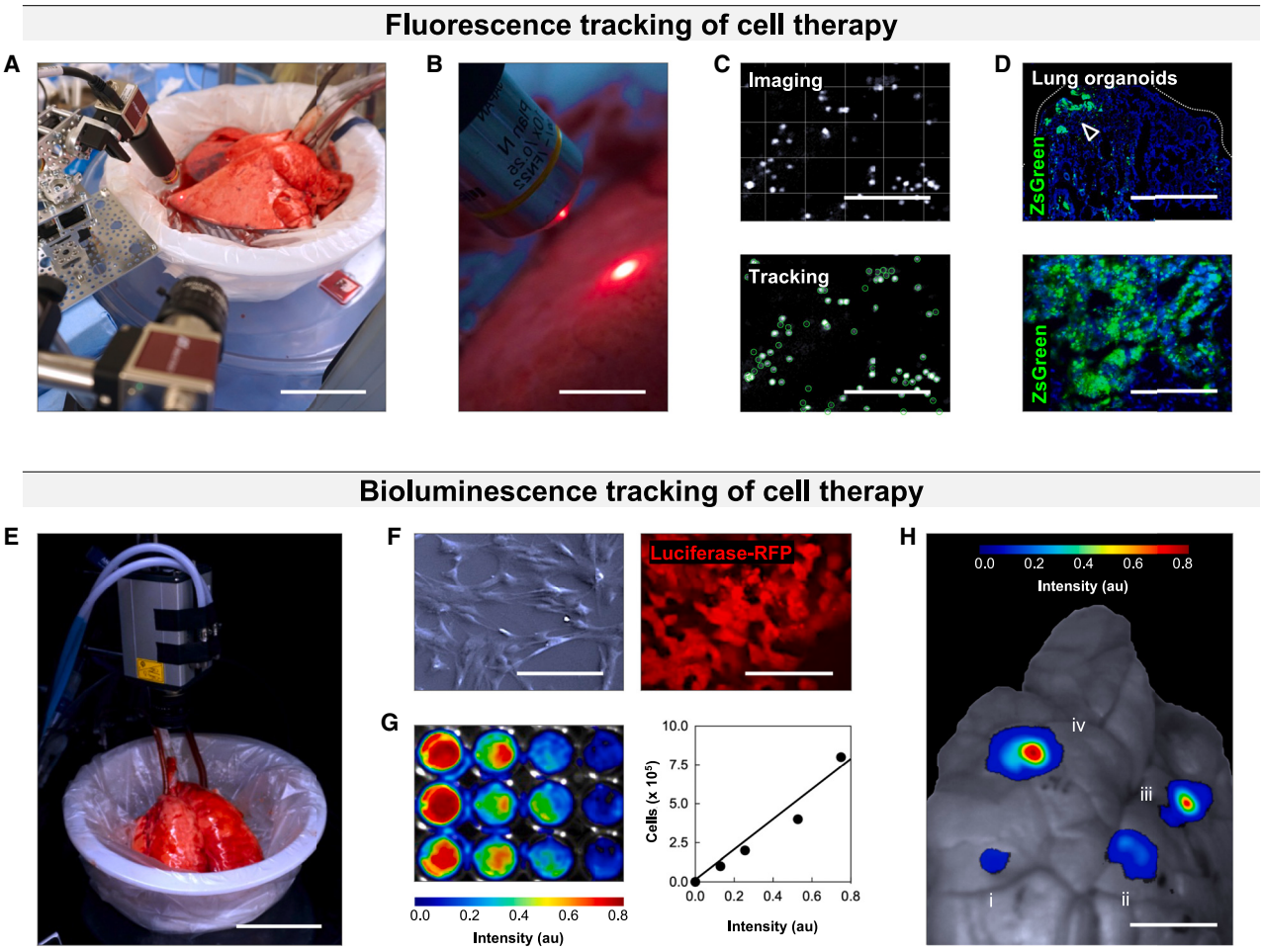

Figure 6. Tracking techniques for therapeutic modalities in *ex vivo* lungs

(A) Custom fluorescence microscopy setup for fluorescence tracking. Scale bar: 10 cm.
(B) Fluorescence microscopy for fluorescence tracking. Scale bar: 1 cm.
(C) Fluorescence imaging and tracking of fluorescent mesenchymal stromal cells using custom software. Scale bar: 250 μm.
(D) Visualization of lung organoids derived from human embryonic stem cells and delivered by transpleural injection. Scale bar: 750 μm.
(E) Custom bioluminescence microscopy setup for bioluminescence tracking. Scale bar: 10 cm.
(F) Expression of luciferase in bioluminescent mesenchymal stromal cells *in vitro*. Scale bar: 100 μm.
(G) Standard curve of bioluminescent mesenchymal stromal cells. au, arbitrary unit.
(H) Bioluminescence tracking of bioluminescent mesenchymal stromal cells delivered by transpleural injection: (i) 1.0×10^5 cells; (ii) 2.5×10^5 cells; (iii) 5.0×10^5 cells; (iv) 1.0×10^6 cells. Scale bar: 1 cm. au, arbitrary unit.

during cross-circulation and were tracked using the transpleural fluorescence imaging system. Post-procedural immunohistochemical staining revealed distributions of cells and cellular aggregates ranging from small clusters (diameter of <50 μm) to large aggregates (diameter of 250–500 μm; Figure 6D). Lung organoids delivered to conducting airways homed to the airway epithelium and appeared to integrate into regions expressing smooth muscle actin and mucin (Figure S7C). Lung organoids delivered bronchoscopically into the respiratory zone demonstrated punctate expression of SPB, indicating the presence of functional type II cells (Figure S7C). These results suggest that upon delivery into *ex vivo* lungs, lung organoids localize throughout the lung parenchyma and adapt in a region-specific manner.

Bioluminescence tracking

To compensate for the limited penetrative depth of transpleural fluorescence imaging, we developed a transpleural bioluminescence imaging system (Figures 6E and S4B). MSCs transfected with luciferase were confirmed to be bioluminescent *in vitro* (Figure 6F), and a standard curve was generated by correlating bioluminescent signal intensity with cell number (Figure 6G). After 18 h of cross-circulation, bioluminescent MSCs were delivered bronchoscopically into distal regions of *ex vivo* swine lungs (controls with no injury). Using a high-resolution, low dark current camera in a customized light-tight dark box fixed to the organ support platform, we obtained real-time, non-invasive bioluminescence images of whole lungs and regional wedge biopsies. The ability to quantify local cell distribution and density with

Please cite this article in press as: Pinezich et al., Theranostic methodology for *ex vivo* donor lung rehabilitation, Med (2025), https://doi.org/10.1016/j.medj.2025.100644

Table 1. Diagnostic modalities for *ex vivo* lung assessment

Diagnostic assessment	Functional parameter assessed	Time required, min
Airway		
Bronchoscopy	airway edema, erythema, secretions	15
Bronchoresponse	airway smooth muscle tone	15
Airway cilia motility	mucociliary clearance	15
Cytopathology (BAL fluid)	airway cellular infiltration	30
Total protein (BAL fluid)	broncho/alveolar barrier integrity	30
Airway inflammation (BAL fluid)	airway inflammatory cytokine concentrations	>60
Airway cultures (BAL fluid)	airway bacterial and fungal infection	>60
Parenchyma		
Surface temperature	regional tissue perfusion	5
Oxygenation test	arterial and/or venous oxygen	5
Ventilation test	arterial and/or venous carbon dioxide	5
Dynamic compliance	pulmonary compliance	5
Lung weight	pulmonary edema	5
Global perfusion	pulmonary vascular perfusion	15
Regional perfusion	pulmonary vascular perfusion	15
Vasoresponse	vascular smooth muscle tone	15
Surfactant uptake	type II pneumocyte function	30
Cell viability	parenchymal cell viability	>60
Metabolic activity	parenchymal cell metabolism	>60

BAL, bronchoalveolar lavage.

this imaging approach was verified by varying cell dose and correlating signal intensity and distribution with bright-field overlay of wedge biopsies (Figure 6H). To gauge the advantage of bioluminescence imaging, standard penetration depths for conventional modalities (bright-field, fluorescence) were compared, demonstrating that bioluminescence imaging has a 20- to 120-fold greater penetration depth. Bioluminescence imaging in *ex vivo* donor lungs can thus enable further quantitative visualization of cell density and distribution throughout approximately 50% of total lung volume at end expiration.

DISCUSSION

In this Resource article, we report the first theranostic methodology for *ex vivo* lung rehabilitation on cross-circulation, with detailed technical descriptions of diagnostic evaluations, therapeutic deliveries, and real-time, non-invasive tracking of cells in *ex vivo* donor lungs. Similar to patients awaiting lung transplant who are supported on extracorporeal membrane oxygenation as a bridge to transplant, injured donor organs could be supported on cross-circulation and rehabilitated for use in transplant. Toward that ultimate goal, we developed a theranostic methodology for *ex vivo* lung rehabilitation that is applicable to both translational research and current clinical practice. This compilation of fundamental diagnostic and therapeutic modalities that have been developed and are now available yields high-resolution tissue, cell, and molecular insights that can facilitate risk assessment, inform clinical decision-making, and enable rehabilitation of injured donor lungs that could be recovered for transplant.

Clinical evaluation of donor lungs for transplant involves assessments of gross appearance (visual inspection), airway health (bronchoscopy), radiography (chest X-ray, computed tomography), donor history, compliance, and gas exchange capacity (PaO_2/FiO_2). Notably, failure to meet all acceptable lung donor criteria (Table S1) does not necessarily preclude organ utilization for an appropriate recipient. According to the International Society for Heart and Lung Transplantation, "When offered donor organs, the transplant team should make a decision to accept or decline on the basis of a combination of clinical experience, center experience, and clinical knowledge, including the acuity of the recipient."[33] Many donor lungs that present with potentially reversible injury at the time of procurement are declined for transplantation, as both the time frame to evaluate and ability to rehabilitate injured lungs *ex vivo* remain constrained by the intrinsic limitations of isolated EVLP, which is the current standard of care for machine perfusion of lungs. Application of the theranostic methodology during cross-circulation could offer significant advantages, including (1) prolonged assessment of *ex vivo* donor lungs over 12–100 h, (2) recovery of donor lungs meeting extended criteria (e.g., aspiration pneumonitis, donor age greater than 55 years), (3) improved logistical coordination at transplant centers, and (4) reduced risk of post-operative complications.

We report a series of rapid, point-of-care diagnostic assessments of *ex vivo* lungs that include clinically established modalities (e.g., bronchoscopy, radiography, blood gas analysis) and emerging modalities (e.g., thermography, lung weight, metabolic analysis) (Table 1). Correlation of functional parameters assessed during *ex vivo* rehabilitation with transplant outcomes would help improve risk assessment for recipients. Previous

studies have correlated surface temperature and weight of *ex vivo* lungs with transplant suitability and outcomes[10–12,14] and have shown that assessment of lung metabolic activity after transplant can aid in differential diagnosis of CLAD phenotypes.[24] Thrombi, which are associated with graft failure after transplantation and are difficult to detect by current donor lung assessments, could be identified using the global and/or regional tissue perfusion imaging modalities reported herein.[14] Across the field of organ transplantation, advanced techniques, including machine learning and bioinformatics analysis,[34,35] allograft phenotyping,[36,37] automated histological classification,[36,38] biomarker screening,[39–41] and gene expression and molecular profiling,[42,43] can help inform further development and expansion of the theranostic methodology.

In addition to informing donor organ selection, diagnostic modalities inform the use of established and emerging therapeutic interventions (e.g., delivery of cells, drugs, exosomes, genes, organoids, RNA transcripts, surfactant) to accelerate *ex vivo* lung rehabilitation (Table S2). We also investigated several emerging interventions, including MSC delivery, which has been shown to increase mitochondrial transfer[44–46] and decrease inflammation in *ex vivo* lungs,[30,31,47,48] and lung organoid delivery, which has been proposed as a regenerative cell-based therapy.

We demonstrated bronchoscopic and transpleural delivery strategies to direct cell and organoid delivery to separate targeted regions of *ex vivo* lungs during cross-circulation. Interestingly, robust MSC viability and localization along the respiratory epithelium and within the interstitium were observed after 36 h of cross-circulation (Figure S7A). We also delivered human lung organoids[32,49] into the airways and parenchyma, where expression of region-specific functional markers (e.g., MUC5B in airways, SFB in alveoli) was confirmed (Figure S7C). Lung organoids derived from human induced pluripotent stem cells represent a particularly promising therapeutic approach, as they offer potential for an abundant supply of patient-specific therapeutic cells that could be used for personalized modifications of donor grafts, such as immunogenic priming of donor lungs to recipient antigens. The theranostic methodology could also accommodate development of other therapeutic modalities, including cell, gene, and RNA therapies for *ex vivo* organ rehabilitation.

Real-time, non-destructive tracking of cell-based deliverables is an important aspect of therapeutic interventions in *ex vivo* lungs. To monitor the location, status, and effects of different cell-based therapies, we built custom platforms for transpleural fluorescence and bioluminescence imaging of *ex vivo* lungs. We demonstrated the use of transpleural fluorescence imaging for high-magnification visualization of fluorescent cells in the lung airways and parenchyma. Furthermore, we developed an image-based cell counting algorithm that automatically quantifies cell number after delivery into *ex vivo* lungs, without interrupting mechanical ventilation (Data S1).

Transpleural fluorescence microscopy enables visualization of fluorescent deliverables *in situ*, but is limited by low penetration depth and high autofluorescence. To overcome these limitations, we developed a bioluminescence imaging system to visualize bioluminescent therapeutic cells in *ex vivo* lungs. Bioluminescence imaging offers real-time, quantitative analysis without autofluorescence and with significantly increased penetration depth, enabling visualization of up to approximately 50% of the total lung volume at end expiration, compared to less than 10% of the total lung volume that can be visualized with fluorescence imaging. Expression of luciferase after delivery indicates cell viability, and bioluminescent signal intensity can be precisely quantified to monitor cell location, density, and proliferation.

Limitations of the study

This study was designed to establish a developmental framework for the practical implementation of diagnostic and therapeutic modalities in *ex vivo* lungs during cross-circulation and isolated EVLP. For emerging diagnostic and therapeutic modalities, standardized methods and clinical protocols remain to be established. The set of modalities reported here should not be considered comprehensive, but rather as an initial foundation to build upon through additional technical development and validation across more donor organs and injury types. To that end, a variety of novel modalities are in various stages of development but could be applied to the theranostic methodology in the future, including the use of artificial intelligence (AI) for donor lung optimization,[34] digital auscultation for sound-based analysis of pulmonary air leak,[50] digital finger for compression-based assessment of lung tissue stiffness,[51,52] bioimpedance for measuring epithelial barrier integrity and edema,[53] near-infrared deep tissue imaging,[54] and AI-based smart tracking.

Notably, cross-circulation of human donor organs with support swine involves important ethical considerations regarding animal use, patients, and public health. Prior to the use of cell-based therapies (e.g., cells, exosomes, organoids) in donor lungs for transplantation, all applicable regulatory requirements pertaining to safety and efficacy must be satisfied. Careful consideration must also be given to how interventions in *ex vivo* lungs, including cell-based therapies, integrate within current care pathways, including standard practices for donor organ selection, allocation, and preservation. Future studies will need to investigate how functional assessments in *ex vivo* lungs correlate with long-term graft function and transplant outcomes across lung injury types, potentially revealing novel prognostic biomarkers.

Future perspective

We envision that donor organs not initially accepted for transplantation can be rehabilitated and recovered in an organ intensive care unit (ICU) setting, where a fully developed theranostic methodology for *ex vivo* organ rehabilitation is applied during cross-circulation. Therapeutic interventions could be tailored to treat specific injuries or to prime the organ for transplantation into the recipient as a new form of personalized medicine. The use of cross-circulation and isolated EVLP by an increasing number of groups around the world offers the opportunity to improve and expand the theranostic methodology for *ex vivo* rehabilitation of lungs and potentially other organs, including hearts, kidneys, and livers.[55]

RESOURCE AVAILABILITY

Lead contact

Requests for resources, reagents, and/or additional information should be directed to and will be fulfilled by the lead contact, Gordana Vunjak-Novakovic (gv2131@columbia.edu).

Materials availability

This study did not generate new unique reagents.

Data and code availability

Data

All data reported in this paper are available from the lead contact upon request.

Code

All original code reported in this paper is available from the lead contact upon request.

Other

Any additional information required to reanalyze the data reported in this paper is available from the lead contact upon request.

ACKNOWLEDGMENTS

The authors would like to thank the following collaborators for their contributions to this study: Columbia University Institute of Comparative Medicine veterinary staff, including A. Romanov, R. Donocoff, A. Hubbard, S. Robertson, R. Ober, A. McLuckie, N. Herndon, D. Ordanes, and A. Rivas; Herbert Irving Comprehensive Cancer Center Molecular Pathology Shared Resources, including T. Wu and D. Sun for histology services; N. Cardwell, S. Chicotka, K. Fung, A. Griesemer, S.X.L. Huang, C. Marboe, D. Queen, M. Salna, M. Simpson, J. Stokes, J. Talackine, Y. Tipograf, A. Tumen, and R. Ukita; and S. Pistilli and S. Halligan for administrative support. The authors gratefully acknowledge funding support from the National Institutes of Health (P41 EB027062 to G.V.-N., R01HL120046 to G.V.-N. and H.-W.S., and U01HL134760 to H.-W.S. and G.V.-N.), the Cystic Fibrosis Foundation (VUNJAK23XX0 to G.V.-N., J.K., and M.B.), the Mrs. Shelley F. Kleiner and Dr. Fredric Kleiner Fund (to M.B.), the David M. Livingston Lung Transplant Memorial Fund (to M.B.), and the Cardiothoracic Research Fund (to M.B.).

AUTHOR CONTRIBUTIONS

M.R.P., J.D.O., B.A.G., A.E.H., M.B., and G.V.-N. planned the studies. M.R.P., J.D.O., B.A.G., J.K., O.F.V., S.P.M., Y.-W.C., A.E.H., A.K., M.F., K.M.C., H.M.W., J.V.H., and M.B. performed the experiments. M.R.P., J.D.O., B.A.G., J.K., O.F.V., S.P.M., Y.-W.C., A.E.H., A.K., M.F., K.M.C., H.M.W., and H.-W.S. analyzed the data and performed the statistical analyses. M.R.P., J.D.O., and B.A.G. had unrestricted access to the data and co-wrote the first draft of the manuscript. J.K., O.F.V., S.P.M., Y.-W.C., A.E.H., A.K., M.F., K.M.C., H.M.W., H.-W.S., M.B., and G.V.-N. reviewed and revised the manuscript. All authors agreed to submit the manuscript, read and approved the final draft, and take responsibility for its contents, including the accuracy of the data.

DECLARATION OF INTERESTS

J.D.O., B.A.G., M.B., and G.V.-N. are co-inventors on a patent (US 11,968,974) describing cross-circulation. M.B. is a co-inventor on a patent application (US20240156081A1) describing cross-circulation. J.D.O. is an officer at Xylyx Bio, a company with a license for cross-circulation. J.D.O., M.B., and G.V.-N. own stock in Xylyx Bio.

STAR★METHODS

Detailed methods are provided in the online version of this paper and include the following:

SUPPLEMENTAL INFORMATION

Supplemental information can be found online at https://doi.org/10.1016/j.medj.2025.100644.

Received: July 15, 2024
Revised: October 15, 2024
Accepted: March 5, 2025
Published: March 27, 2025

REFERENCES

1. Verleden, S., Martens, A., Heigl, T., Bellon, H., Vandermeulen, E., Vos, R., Verschakelen, J., Coudyzer, W., Van Raemdonck, D., Neyrinck, A., and Vanaudenaerde, B. (2016). A post-hoc analysis of donor lungs declined for transplantation. Eur. Respir. J. *48*, OA3337. https://doi.org/10.1183/13993003.congress-2016.OA3337.
2. Pinezich, M., and Vunjak-Novakovic, G. (2019). Bioengineering approaches to organ preservation ex vivo. Exp. Biol. Med. *244*, 630–645. https://doi.org/10.1177/1535370219834498.
3. Cypel, M., Yeung, J.C., Donahoe, L., Chen, M., Zamel, R., Hoetzenecker, K., Yasufuku, K., de Perrot, M., Pierre, A.F., Waddell, T.K., and Keshavjee, S. (2020). Normothermic ex vivo lung perfusion: Does the indication impact organ utilization and patient outcomes after transplantation? J. Thorac. Cardiovasc. Surg. *159*, 346–355.e1. https://doi.org/10.1016/j.jtcvs.2019.06.123.
4. Peel, J.K., Keshavjee, S., Naimark, D., Liu, M., Del Sorbo, L., Cypel, M., Barrett, K., Pullenayegum, E.M., and Sander, B. (2023). Determining the impact of ex-vivo lung perfusion on hospital costs for lung transplantation: A retrospective cohort study. J. Heart Lung Transplant. *42*, 356–367. https://doi.org/10.1016/j.healun.2022.10.016.
5. Guenthart, B.A., O'Neill, J.D., Kim, J., Queen, D., Chicotka, S., Fung, K., Simpson, M., Donocoff, R., Salna, M., Marboe, C.C., et al. (2019). Regeneration of severely damaged lungs using an interventional cross-circulation platform. Nat. Commun. *10*, 1985. https://doi.org/10.1038/s41467-019-09908-1.
6. Hozain, A.E., Tipograf, Y., Pinezich, M.R., Cunningham, K.M., Donocoff, R., Queen, D., Fung, K., Marboe, C.C., Guenthart, B.A., O'Neill, J.D., et al. (2020). Multiday maintenance of extracorporeal lungs using cross-circulation with conscious swine. J. Thorac. Cardiovasc. Surg. *159*, 1640–1653.e18. https://doi.org/10.1016/j.jtcvs.2019.09.121.
7. Hozain, A.E., O'Neill, J.D., Pinezich, M.R., Tipograf, Y., Donocoff, R., Cunningham, K.M., Tumen, A., Fung, K., Ukita, R., Simpson, M.T., et al. (2020). Xenogeneic cross-circulation for extracorporeal recovery of injured human lungs. Nat. Med. *26*, 1102–1113. https://doi.org/10.1038/s41591-020-0971-8.
8. O'Neill, J.D., Guenthart, B.A., Kim, J., Chicotka, S., Queen, D., Fung, K., Marboe, C., Romanov, A., Huang, S.X.L., Chen, Y.-W., et al. (2017). Cross-circulation for extracorporeal support and recovery of the lung. Nat. Biomed. Eng. *1*, 0037. https://doi.org/10.1038/s41551-017-0037.

9. Kelly Wu, W., Guenthart, B.A., O'Neill, J.D., Hozain, A.E., Tipograf, Y., Ukita, R., Stokes, J.W., Patel, Y.J., Pinezich, M., Talackine, J.R., et al. (2023). Technique for xenogeneic cross-circulation to support human donor lungs ex vivo. J. Heart Lung Transplant. *42*, 335–344. https://doi.org/10.1016/j.healun.2022.11.002.

10. Kosaka, R., Sakota, D., Niikawa, H., Ohuchi, K., Arai, H., McCurry, K.R., and Okamoto, T. (2022). Lung thermography during the initial reperfusion period to assess pulmonary function in cellular ex vivo lung perfusion. Artif. Organs *46*, 1522–1532. https://doi.org/10.1111/aor.14219.

11. Okamoto, T., Ayyat, K.S., Sakanoue, I., Niikawa, H., Said, S.A., Ahmad, U., Unai, S., Bribriesco, A., Elgharably, H., Budev, M.M., et al. (2022). Clinical significance of donor lung weight at procurement and during ex vivo lung perfusion. J. Heart Lung Transplant. *41*, 818–828. https://doi.org/10.1016/j.healun.2022.02.011.

12. Okamoto, T., Niikawa, H., Wheeler, D., Soliman, B., Ayyat, K.S., Itoda, Y., Farver, C.F., and McCurry, K.R. (2021). Significance of Lung Weight in Cellular Ex Vivo Lung Perfusion. J. Surg. Res. *260*, 190–199. https://doi.org/10.1016/j.jss.2020.11.069.

13. Chao, B.T., McInnis, M.C., Sage, A.T., Yeung, J.C., Cypel, M., Liu, M., Wang, B., and Keshavjee, S. (2024). A radiographic score for human donor lungs on ex vivo lung perfusion predicts transplant outcomes. J. Heart Lung Transplant. *43*, 797–805. https://doi.org/10.1016/j.healun.2024.01.004.

14. Motoyama, H., Chen, F., Hijiya, K., Kondo, T., Ohata, K., Takahashi, M., Yamada, T., Sato, M., Aoyama, A., and Date, H. (2015). Novel thermographic detection of regional malperfusion caused by a thrombosis during ex vivo lung perfusion. Interact. Cardiovasc. Thorac. Surg. *20*, 242–247. https://doi.org/10.1093/icvts/ivu386.

15. Andreasson, A.S., Karamanou, D.M., Gillespie, C.S., Özalp, F., Butt, T., Hill, P., Jiwa, K., Walden, H.R., Green, N.J., Borthwick, L.A., et al. (2017). Profiling inflammation and tissue injury markers in perfusate and bronchoalveolar lavage fluid during human ex vivo lung perfusion. European Journal of Cardio-Thoracic Surgery *51*, 577–586. https://doi.org/10.1093/ejcts/ezw358.

16. Stanbrook, M.B., and Kesten, S. (1999). Bronchial Hyperreactivity after Lung Transplantation Predicts Early Bronchiolitis Obliterans. Am. J. Respir. Crit. Care Med. *160*, 2034–2039. https://doi.org/10.1164/ajrccm.160.6.9801037.

17. Suryadinata, R., Levin, K., Holsworth, L., Paraskeva, M., and Robinson, P. (2021). Airway cilia recovery post lung transplantation. Immun. Inflamm. Dis. *9*, 1716–1723. https://doi.org/10.1002/iid3.527.

18. Verleden, S.E., Martens, A., Ordies, S., Neyrinck, A.P., Van Raemdonck, D.E., Verleden, G.M., Vanaudenaerde, B.M., and Vos, R. (2018). Immediate post-operative broncho-alveolar lavage IL-6 and IL-8 are associated with early outcomes after lung transplantation. Clin. Transplant. *32*, e13219. https://doi.org/10.1111/ctr.13219.

19. Terragni, P.P., Fanelli, V., Boffini, M., Filippini, C., Cappello, P., Ricci, D., Del Sorbo, L., Faggiano, C., Brazzi, L., Frati, G., et al. (2016). Ventilatory Management During Normothermic Ex Vivo Lung Perfusion: Effects on Clinical Outcomes. Transplantation *100*, 1128–1135. https://doi.org/10.1097/TP.0000000000000929.

20. Tague, L.K., Bedair, B., Witt, C., Byers, D.E., Vazquez-Guillamet, R., Kulkarni, H., Alexander-Brett, J., Nava, R., Puri, V., Kreisel, D., et al. (2021). Lung protective ventilation based on donor size is associated with a lower risk of severe primary graft dysfunction after lung transplantation. J. Heart Lung Transplant. *40*, 1212–1222. https://doi.org/10.1016/j.healun.2021.06.016.

21. Niroomand, A., Qvarnström, S., Stenlo, M., Malmsjö, M., Ingemansson, R., Hyllén, S., and Lindstedt, S. (2022). The role of mechanical ventilation in primary graft dysfunction in the postoperative lung transplant recipient: A single center study and literature review. Acta Anaesthesiol. Scand. *66*, 483–496. https://doi.org/10.1111/aas.14025.

22. Ficial, B., Vasques, F., Zhang, J., Whebell, S., Slattery, M., Lamas, T., Daly, K., Agnew, N., and Camporota, L. (2021). Physiological Basis of Extracorporeal Membrane Oxygenation and Extracorporeal Carbon Dioxide Removal in Respiratory Failure. Membranes *11*, 225. https://doi.org/10.3390/membranes11030225.

23. Himmat, S., Alzamil, A., Aboelnazar, N., Hatami, S., White, C., Dromparis, P., Mengel, M., Freed, D., and Nagendran, J. (2018). A Decrease in Hypoxic Pulmonary Vasoconstriction Correlates With Increased Inflammation During Extended Normothermic Ex Vivo Lung Perfusion. Artif. Organs *42*, 271–279. https://doi.org/10.1111/aor.13017.

24. Verleden, S.E., Gheysens, O., Goffin, K.E., Vanaudenaerde, B.M., Verbeken, E.K., Weynand, B., Van Raemdonck, D.E., Verleden, G.M., and Vos, R. (2019). Role of 18F-FDG PET/CT in Restrictive Allograft Syndrome After Lung Transplantation. Transplantation *103*, 823–831. https://doi.org/10.1097/TP.0000000000002393.

25. Capuzzimati, M., Hough, O., and Liu, M. (2022). Cell death and ischemia-reperfusion injury in lung transplantation. J. Heart Lung Transplant. *41*, 1003–1013. https://doi.org/10.1016/j.healun.2022.05.013.

26. Nakajima, D., Liu, M., Ohsumi, A., Kalaf, R., Iskender, I., Hsin, M., Kanou, T., Chen, M., Baer, B., Coutinho, R., et al. (2017). Lung Lavage and Surfactant Replacement During Ex Vivo Lung Perfusion for Treatment of Gastric Acid Aspiration-Induced Donor Lung Injury. J. Heart Lung Transplant. *36*, 577–585. https://doi.org/10.1016/j.healun.2016.11.010.

27. D'Ovidio, F., Floros, J., Aramini, B., Lederer, D., DiAngelo, S.L., Arcasoy, S., Sonett, J.R., Robbins, H., Shah, L., Costa, J., and Urso, A. (2020). Donor surfactant protein A2 polymorphism and lung transplant survival. Eur. Respir. J. *55*, 1900618. https://doi.org/10.1183/13993003.00618-2019.

28. Belhaj, A., Boven, C., Dewachter, L., Ruiz Patino, M., Sokolow, Y., and Rondelet, B. (2017). Influence of Donor Lung Surfactant-A and -B Protein Expression on the Development of Primary Graft Dysfunction After Lung Transplantation: A Pilot Study. Ann. Transplant. *22*, 361–369. https://doi.org/10.12659/aot.903313.

29. Lee, J.W., Fang, X., Gupta, N., Serikov, V., and Matthay, M.A. (2009). Allogeneic human mesenchymal stem cells for treatment of E. coli endotoxin-induced acute lung injury in the ex vivo perfused human lung. Proc. Natl. Acad. Sci. USA *106*, 16357–16362. https://doi.org/10.1073/pnas.0907996106.

30. Nakajima, D., Watanabe, Y., Ohsumi, A., Pipkin, M., Chen, M., Mordant, P., Kanou, T., Saito, T., Lam, R., Coutinho, R., et al. (2019). Mesenchymal stromal cell therapy during ex vivo lung perfusion ameliorates ischemia-reperfusion injury in lung transplantation. J. Heart Lung Transplant. *38*, 1214–1223. https://doi.org/10.1016/j.healun.2019.07.006.

31. Nykänen, A.I., Mariscal, A., Duong, A., Estrada, C., Ali, A., Hough, O., Sage, A., Chao, B.T., Chen, M., Gokhale, H., et al. (2021). Engineered mesenchymal stromal cell therapy during human lung ex vivo lung perfusion is compromised by acidic lung microenvironment. Mol. Ther. Methods Clin. Dev. *23*, 184–197. https://doi.org/10.1016/j.omtm.2021.05.018.

32. Chen, Y.-W., Huang, S.X., de Carvalho, A.L.R.T., Ho, S.-H., Islam, M.N., Volpi, S., Notarangelo, L.D., Ciancanelli, M., Casanova, J.-L., Bhattacharya, J., et al. (2017). A three-dimensional model of human lung development and disease from pluripotent stem cells. Nat. Cell Biol. *19*, 542–549. https://doi.org/10.1038/ncb3510.

33. Copeland, H., Hayanga, J.W.A., Neyrinck, A., MacDonald, P., Dellgren, G., Bertolotti, A., Khuu, T., Burrows, F., Copeland, J.G., Gooch, D., et al. (2020). Donor heart and lung procurement: A consensus statement. J. Heart Lung Transplant. *39*, 501–517. https://doi.org/10.1016/j.healun.2020.03.020.

34. Sage, A.T., Donahoe, L.L., Shamandy, A.A., Mousavi, S.H., Chao, B.T., Zhou, X., Valero, J., Balachandran, S., Ali, A., Martinu, T., et al. (2023). A machine-learning approach to human ex vivo lung perfusion predicts transplantation outcomes and promotes organ utilization. Nat. Commun. *14*, 4810. https://doi.org/10.1038/s41467-023-40468-7.

35. Raynaud, M., Aubert, O., Divard, G., Reese, P.P., Kamar, N., Yoo, D., Chin, C.-S., Bailly, É., Buchler, M., Ladrière, M., et al. (2021). Dynamic prediction

of renal survival among deeply phenotyped kidney transplant recipients using artificial intelligence: an observational, international, multicohort study. Lancet. Digit. Health *3*, e795–e805. https://doi.org/10.1016/S2589-7500(21)00209-0.

36. Yoo, D., Goutaudier, V., Divard, G., Gueguen, J., Astor, B.C., Aubert, O., Raynaud, M., Demir, Z., Hogan, J., Weng, P., et al. (2023). An automated histological classification system for precision diagnostics of kidney allografts. Nat. Med. *29*, 1211–1220. https://doi.org/10.1038/s41591-023-02323-6.
37. Loupy, A., Aubert, O., Orandi, B.J., Naesens, M., Bouatou, Y., Raynaud, M., Divard, G., Jackson, A.M., Viglietti, D., Giral, M., et al. (2019). Prediction system for risk of allograft loss in patients receiving kidney transplants: international derivation and validation study. Br. Med. J. *366*, l4923. https://doi.org/10.1136/bmj.l4923.
38. Predella, C., Iezza, D., Miller, M.L., Swayne, T., Saqi, A., and Dorrello, N.V. (2023). Standardized Digital Method for Histological Evaluation of Experimental Acute Lung Injury. Am. J. Respir. Cell Mol. Biol. *69*, 596–598. https://doi.org/10.1165/rcmb.2023-0182LE.
39. Duong Van Huyen, J.-P., Tible, M., Gay, A., Guillemain, R., Aubert, O., Varnous, S., Iserin, F., Rouvier, P., François, A., Vernerey, D., et al. (2014). MicroRNAs as non-invasive biomarkers of heart transplant rejection. Eur. Heart J. *35*, 3194–3202. https://doi.org/10.1093/eurheartj/ehu346.
40. Goutaudier, V., Sablik, M., Racapé, M., Rousseau, O., Audry, B., Kamar, N., Raynaud, M., Aubert, O., Charreau, B., Papuchon, E., et al. (2024). Design, cohort profile and comparison of the KTD-Innov study: a prospective multidimensional biomarker validation study in kidney allograft rejection. Eur. J. Epidemiol. *39*, 549–564. https://doi.org/10.1007/s10654-024-01112-w.
41. Demir, Z., Raynaud, M., Aubert, O., Debray, D., Sebagh, M., Duong Van Huyen, J.-P., Del Bello, A., Jolivet, N.C., Paradis, V., Durand, F., et al. (2024). Identification of liver transplant biopsy phenotypes associated with distinct liver biological markers and allograft survival. Am. J. Transplant. *24*, 954–966. https://doi.org/10.1016/j.ajt.2023.12.007.
42. Halloran, P.F., Potena, L., Van Huyen, J.-P.D., Bruneval, P., Leone, O., Kim, D.H., Jouven, X., Reeve, J., and Loupy, A. (2017). Building a tissue-based molecular diagnostic system in heart transplant rejection: The heart Molecular Microscope Diagnostic (MMDx) System. J. Heart Lung Transplant. *36*, 1192–1200. https://doi.org/10.1016/j.healun.2017.05.029.
43. Loupy, A., Lefaucheur, C., Vernerey, D., Chang, J., Hidalgo, L.G., Beuscart, T., Verine, J., Aubert, O., Dubleumortier, S., Duong van Huyen, J.-P., et al. (2014). Molecular microscope strategy to improve risk stratification in early antibody-mediated kidney allograft rejection. J. Am. Soc. Nephrol. *25*, 2267–2277. https://doi.org/10.1681/ASN.2013111149.
44. Huang, T., Lin, R., Su, Y., Sun, H., Zheng, X., Zhang, J., Lu, X., Zhao, B., Jiang, X., Huang, L., et al. (2023). Efficient intervention for pulmonary fibrosis via mitochondrial transfer promoted by mitochondrial biogenesis. Nat. Commun. *14*, 5781. https://doi.org/10.1038/s41467-023-41529-7.
45. Tan, Y.L., Eng, S.P., Hafez, P., Abdul Karim, N., Law, J.X., and Ng, M.H. (2022). Mesenchymal Stromal Cell Mitochondrial Transfer as a Cell Rescue Strategy in Regenerative Medicine: A Review of Evidence in Preclinical Models. Stem Cells Transl. Med. *11*, 814–827. https://doi.org/10.1093/stcltm/szac044.
46. Li, X., Zhang, Y., Yeung, S.C., Liang, Y., Liang, X., Ding, Y., Ip, M.S.M., Tse, H.-F., Mak, J.C.W., and Lian, Q. (2014). Mitochondrial Transfer of Induced Pluripotent Stem Cell–Derived Mesenchymal Stem Cells to Airway Epithelial Cells Attenuates Cigarette Smoke–Induced Damage. Am. J. Respir. Cell Mol. Biol. *51*, 455–465. https://doi.org/10.1165/rcmb.2013-0529OC.
47. Mordant, P., Nakajima, D., Kalaf, R., Iskender, I., Maahs, L., Behrens, P., Coutinho, R., Iyer, R.K., Davies, J.E., Cypel, M., et al. (2016). Mesenchymal stem cell treatment is associated with decreased perfusate concentration of interleukin-8 during ex vivo perfusion of donor lungs after 18-hour preservation. J. Heart Lung Transplant. *35*, 1245–1254. https://doi.org/10.1016/j.healun.2016.04.017.
48. Martens, A., Ordies, S., Vanaudenaerde, B.M., Verleden, S.E., Vos, R., Van Raemdonck, D.E., Verleden, G.M., Roobrouck, V.D., Claes, S., Schols, D., et al. (2017). Immunoregulatory effects of multipotent adult progenitor cells in a porcine ex vivo lung perfusion model. Stem Cell Res. Ther. *8*, 159. https://doi.org/10.1186/s13287-017-0603-5.
49. Huang, S.X.L., Islam, M.N., O'Neill, J., Hu, Z., Yang, Y.-G., Chen, Y.-W., Mumau, M., Green, M.D., Vunjak-Novakovic, G., Bhattacharya, J., and Snoeck, H.W. (2014). Efficient generation of lung and airway epithelial cells from human pluripotent stem cells. Nat. Biotechnol. *32*, 84–91. https://doi.org/10.1038/nbt.2754.
50. Pinezich, M.R., Mir, S.M., Reimer, J.A., Kaslow, S.R., Chen, J., Guenthart, B.A., Bacchetta, M., O'Neill, J.D., Vunjak-Novakovic, G., and Kim, J. (2023). Sound-guided assessment and localization of pulmonary air leak. Bioengineering & Translational Medicine *n/a*. Bioeng. Transl. Med. *8*, e10322. https://doi.org/10.1002/btm2.10322.
51. Mir, M., Chen, J., Patel, A., Pinezich, M.R., Guenthart, B.A., Vunjak-Novakovic, G., and Kim, J. (2024). A Minimally Invasive Robotic Tissue Palpation Device. IEEE Trans. Biomed. Eng. *71*, 1958–1968. https://doi.org/10.1109/TBME.2024.3357293.
52. Chen, J., Mir, M., Pinezich, M.R., O'Neill, J.D., Guenthart, B.A., Bacchetta, M., Vunjak-Novakovic, G., Huang, S.X.L., and Kim, J. (2021). Non-destructive vacuum-assisted measurement of lung elastic modulus. Acta Biomater. *131*, 370–380. https://doi.org/10.1016/j.actbio.2021.06.037.
53. Chen, J., Mir, S.M., Hudock, M.R., Pinezich, M.R., Chen, P., Bacchetta, M., Vunjak-Novakovic, G., and Kim, J. (2023). Opto-electromechanical quantification of epithelial barrier function in injured and healthy airway tissues. APL Bioeng. *7*, 016104. https://doi.org/10.1063/5.0123127.
54. Kim, J., Guenthart, B., O'Neill, J.D., Dorrello, N.V., Bacchetta, M., and Vunjak-Novakovic, G. (2017). Controlled delivery and minimally invasive imaging of stem cells in the lung. Sci. Rep. *7*, 13082. https://doi.org/10.1038/s41598-017-13280-9.
55. Wu, W.K., Ukita, R., Patel, Y.J., Cortelli, M., Trinh, V.Q., Ziogas, I.A., Francois, S.A., Mentz, M., Cardwell, N.L., Talackine, J.R., et al. (2023). Xenogeneic cross-circulation for physiological support and recovery of ex vivo human livers. Hepatology *78*, 820–834. https://doi.org/10.1097/HEP.0000000000000357.
56. Sachs, D.H., Leight, G., Cone, J., Schwarz, S., Stuart, L., and Rosenberg, S. (1976). Transplantation in miniature swine. I. Fixation of the major histocompatibility complex. Transplantation *22*, 559–567. https://doi.org/10.1097/00007890-197612000-00004.
57. Vila, O.F., Garrido, C., Cano, I., Guerra-Rebollo, M., Navarro, M., Meca-Cortés, O., Ma, S.P., Engel, E., Rubio, N., and Blanco, J. (2016). Real-Time Bioluminescence Imaging of Cell Distribution, Growth, and Differentiation in a Three-Dimensional Scaffold Under Interstitial Perfusion for Tissue Engineering. Tissue Eng. Part C Methods *22*, 864–872. https://doi.org/10.1089/ten.tec.2014.0421.
58. Bagó, J.R., Aguilar, E., Alieva, M., Soler-Botija, C., Vila, O.F., Claros, S., Andrades, J.A., Becerra, J., Rubio, N., and Blanco, J. (2013). In Vivo Bioluminescence Imaging of Cell Differentiation in Biomaterials: A Platform for Scaffold Development. Tissue Eng. Part A *19*, 593–603. https://doi.org/10.1089/ten.tea.2012.0073.
59. Kaslow, S.R., Reimer, J.A., Pinezich, M.R., Hudock, M.R., Chen, P., Morris, M.G., Kain, M.L., Leb, J.S., Ruzal-Shapiro, C.B., Marboe, C.C., et al. (2022). A clinically relevant model of acute respiratory distress syndrome in human-size swine. Dis. Model. Mech. *15*, dmm049603. https://doi.org/10.1242/dmm.049603.
60. Chen, P., Van Hassel, J., Pinezich, M.R., Diane, M., Hudock, M.R., Kaslow, S.R., Gavaudan, O.P., Fung, K., Kain, M.L., Lopez, H., et al. (2024). Recovery of extracorporeal lungs using cross-circulation with injured recipient swine. J. Thorac. Cardiovasc. Surg. *167*, e106–e130. https://doi.org/10.1016/j.jtcvs.2023.09.032.

61. Chen, Y.-W., Ahmed, A., and Snoeck, H.-W. (2017). Generation of three-dimensional lung bud organoid and its derived branching colonies. Protocol Exchange, 1–8. https://doi.org/10.1038/protex.2017.027.

62. Wu, W.K., Tumen, A., Stokes, J.W., Ukita, R., Hozain, A., Pinezich, M., O'Neill, J.D., Lee, M.J., Reimer, J.A., Flynn, C.R., et al. (2022). Cross-Circulation for Extracorporeal Liver Support in a Swine Model. ASAIO J. *68*, 561–570. https://doi.org/10.1097/MAT.0000000000001543.

63. Guenthart, B.A., O'Neill, J.D., Kim, J., Fung, K., Vunjak-Novakovic, G., and Bacchetta, M. (2019). Cell replacement in human lung bioengineering. J. Heart Lung Transplant. *38*, 215–224. https://doi.org/10.1016/j.healun.2018.11.007.

Please cite this article in press as: Pinezich et al., Theranostic methodology for *ex vivo* donor lung rehabilitation, Med (2025), https://doi.org/10.1016/j.medj.2025.100644

STAR★METHODS

KEY RESOURCES TABLE

REAGENT or RESOURCE	SOURCE	IDENTIFIER
Human donor lungs	Organ procurement organization	N/A
Alprostadil	Medline, Pfizer	NDC: 00009-3169-06
BODIPY FL succinimidyl ester	ThermoFisher Scientific	Cat #: D2184
Bovine lipid extract surfactant	BLES Biochemicals	ATC Code: R07AA02
Buprenorphine hydrochloride	Patterson Veterinary	NDC: 42023-179-05
Cefazolin	Covetrus, WG Critical Care	NDC: 44567-707-25
CFSE	Abcam	Cat #: ab113853
DAPI	ThermoFisher Scientific	Cat #: 62248
Fentanyl citrate	Covetrus, Hikma Pharmaceuticals	NDC: 0641-6030-01
Heparin	Covetrus, Sagent	NDC: 25021-400-30
Isoflurane	Covetrus	NDC: 11695-0677-71
Methacholine	McKesson, Methapharm	NDC: 64281-100-06
Methylprednisolone	Covetrus, Pfizer	NDC: 0009-0018-20
Midazolam	Covetrus, Avet Pharma	NDC: 23155-0601-41
Mycophenolate	Roche	NDC: 0004-0298-09
Omnipaque	Henry Schein Medical	NDC: 0407-1412-30
Perfadex	XVIVO	Ref #: 19850
Phenylephrine	Covetrus, Hikma Pharmaceuticals	NDC: 0641-6142-25
Renilla luciferase substrate	Promega	Cat #: P1231
Tacrolimus	American Health Pack., McKesson	NDC: 68084-451-01
Telazol	Covetrus, Zoetis	Ref #: 10004135
Critical commercial assays		
AlamarBlue Cell Viability Assay	ThermoFisher Scientific	Cat #: DAL1025
IL-1β ELISA Kit	ThermoFisher Scientific	Cat #: ESIL1B
IL-6 ELISA Kit	ThermoFisher Scientific	Cat #: ESIL6
IL-10 ELISA Kit	ThermoFisher Scientific	Cat #: KSC0101
Pierce Coomassie Bradford Protein Assay Kit	ThermoFisher Scientific	Cat #: 23200
TNF-α ELISA Kit	ThermoFisher Scientific	Cat #: KSC3012
Experimental models: Cell lines		
Human: HEK-293FT cells	ThermoFisher Scientific	Cell line #: 293FT
Human: Pluripotent stem cells (passage 17–28)	Chen et al.,[32] Huang et al.[49]	Cell line #: RUES2
Human: Primary mesenchymal stromal cells	Lonza	Cat #: PT-2501
Experimental models: Organisms/strains		
Miniature swine (age: 5–7 months, weight: 38–70 kg)	Sachs et al.[56]	N/A
Yorkshire swine (age: 5–8 months, weight: 61–64 kg)	Animal Biotech Industries	N/A
Recombinant DNA		
Lentiviral vector: *Renilla reniformis* luciferase	Villa et al.,[57] Bagó et al.[58]	CMV:hRLuc:mRFP:ttk
Software and algorithms		
DICOM Viewer	MicroDICOM	microdicom.com
ImageJ	NIH	ImageJ.net/software/fiji
MATLAB	Mathworks	mathworks.com/products
NIS Elements Advanced Research	Nikon	microscope.healthcare.nikon.com/products/software/nis-elements/software-resources

(*Continued on next page*)

Continued

REAGENT or RESOURCE	SOURCE	IDENTIFIER
Prism (version 10)	GraphPad	graphpad.com/features
Research IR	FLIR	flir.com/products/flir-research-studio/?vertical=rd%20science&segment=solutions
Other		
Blood gas analyzer	Heska	Model #: Element POC 5409
CMOS camera	Andor	Model #: Zyla 5.5
Digital scale	WeighMax	Model #: W-4830
Flexible bronchoscope	Ambu	Model #: aScope 3
Fluorescence microscope	Olympus	Model #: IX 81
Laser speckle contrast imager	RWD Life Sciences	Model #: RFLSI-ZW
Light microscope	Olympus	Model #: FSX100
Nebulizer	Aerogen	Model #: Solo 10-356
Thermal camera	FLIR	Model #: T430sc
Whole blood coagulation tester	Accriva Diagnostics	Model #: HemoChron 000ELITE
X-ray mobile unit	United Radiology Systems	Model #: PXP-16HF

EXPERIMENTAL MODEL AND STUDY PARTICIPANT DETAILS

Study design

The study objective was to establish a methodology of diagnostic and therapeutic modalities for rehabilitation of *ex vivo* lungs with severe acute injuries that often render donor lungs unacceptable for transplantation. Such a methodology has not been previously described, and is needed to inform development of guidelines, protocols, and standardized practices for *ex vivo* lung rehabilitation. All modalities were developed in the experimental setting of cross-circulation or isolated *ex vivo* lung perfusion (EVLP) of swine lungs or human donor lungs that were declined for transplantation and consented for research use (Table S3).

To develop the methodology, we utilized *ex vivo* lungs (n = 23; 17 injured, 6 control) with multi-focal contusion (n = 6, human), gastric aspiration injury (n = 8, swine), ischemia–reperfusion injury (n = 3, swine), and no injury (n = 6, swine). Control lungs were used to establish benchmarks and reference ranges. Development of diagnostic and therapeutic modalities was driven by the need for (*i*) robust qualitative and quantitative indicators of organ condition and function during rehabilitation, and (*ii*) delivery and tracking techniques that can facilitate therapeutic treatment of *ex vivo* lungs. Each modality is described in sufficient detail so that other investigators may adapt and/or further develop the methodology to improve *ex vivo* lung rehabilitation. All samples were analyzed as technical replicates in triplicate. Representative results in the form of a longitudinal comparison between two timepoints (e.g., baseline versus endpoint) or from a single timepoint (e.g., midpoint, endpoint) from exemplary cases are reported for each modality.

All donor organ procurements and experimental procedures were performed under protocols approved by the Institutional Review Board at Columbia University Irving Medical Center and Vanderbilt University Medical Center. All animal care and experimental procedures were performed under protocols approved by the Institutional Animal Care and Use Committee at Columbia University Irving Medical Center and Vanderbilt University Medical Center, and conducted in accordance with the U.S. National Research Council of the National Academies *Guide for the Care and Use of Laboratory Animals, Eighth Edition*.

Human donor lungs

Human donor lungs (n = 6) declined for transplantation and consented for research use were procured from deceased donors (2 female, 4 male) with a median age of 29 years (range: 18–45 years) after brain death or circulatory death (Table S4). Lungs were procured in coordination with organ procurement organizations, and organ donor data were obtained under protocols approved by the Institutional Review Board at Columbia University Irving Medical Center (CUIMC) and Vanderbilt University Medical Center (VUMC). Information on gender and socioeconomic status was not collected. Lung procurements were performed by experienced surgeons using standard techniques in coordination with other teams deployed for organ procurement for clinical transplantation. Inclusion/exclusion criteria: Lungs with pulmonary contusion, edema, and/or consolidation were included in the study. Lungs with bronchoscopic or radiographic evidence of severe pneumonia, anticipated cold ischemia time exceeding 36 h, and/or history of human immunodeficiency virus and hepatitis B/C were excluded from the study.

Lungs meeting study criteria were procured as previously described.[7,9] Lungs were flushed *in situ* before explant and carefully mobilized to prevent disruption of the visceral pleura and subsequent air leak or bleeding during procurement. The trachea, pulmonary artery, and left atrial cuff were retained as long as possible to facilitate *ex vivo* cannulation. In cases where the heart was

procured for transplantation by other teams, reconstruction of the left atrial cuff and/or pulmonary artery was required to facilitate *ex vivo* cannulation, which utilized donor pericardium, descending thoracic aorta, and/or polyethylene terephthalate grafts as previously described.[7] Lungs were flushed on a sterile back table with 1 L low-potassium dextran organ preservation solution (Perfadex, XVIVO) at 4°C retrograde under gravity drainage at 30 cmH_2O and placed in a sterile isolation bag (Steri-Drape, 3M) with organ preservation solution at 4°C. The bag containing the lungs was closed, secured, and placed in a second sterile isolation bag with sterile ice, which was then closed, secured, and placed in a third sterile isolation bag to maintain sterility. Lungs were transported on ice at 4°C to the experimental research facility, cannulated, placed on cross-circulation, and used to develop diagnostic and therapeutic modalities.

Animals

Forty (40) swine were used in this study: seventeen (17) swine lung donors and twenty-three (23) support swine. Of the seventeen swine lung donors, three (3) were wildtype Yorkshire swine, and fourteen (14) were miniature swine from a herd of partially-inbred swine with well-defined major histocompatibility complex loci. Selective breeding methods and immunogenetic characteristics of this herd have been previously described.[56] As experimental xenogeneic cross-circulation procedures were conducted at sites in Columbia University and Vanderbilt University, the study received approvals from the Institutional Animal Care and Use Committee at both Columbia University and Vanderbilt University. All animal care and procedures were conducted in accordance with the US National Research Council of the National Academies *Guide for the Care and Use of Laboratory Animals, Eighth Edition*. An overview of all *ex vivo* lungs and support swine used in this study is in Table S3. Swine type, sex, age, and median weight are specified for each experimental swine model (gastric aspiration injury, ischemia–reperfusion injury, no injury) and for all support swine.

Gastric aspiration injury

A swine model of gastric aspiration was used to induce severe aspiration pneumonitis, an acute lung injury that often renders donor lungs unacceptable for transplantation. Miniature swine from a herd of partially inbred swine with well-defined major histocompatibility complex loci were used.[56] Swine lungs (n = 8) were procured from male swine age 5–7 months with a median weight of 39 kg (range: 31–54 kg).

Gastric contents were procured from six swine and standardized as previously described.[5,59,60] Swine were fasted for 12 h then sedated. An orogastric tube (16 Fr) was inserted and engaged to suction. Gastric contents were collected, mixed, strained through surgical gauze to remove large particulates, normalized with hydrochloric acid to a standard pH of 2.00 ± 0.05, sterile filtered, aliquotted, stored at −80°C, and thawed immediately before use. Microbial cultures of gastric contents were confirmed negative.

Gastric aspiration injury was induced *in vivo* as previously described.[5] Swine were sedated, anesthetized via intramuscular induction with Telazol (5 mg/kg) and buprenorphine hydrochloride (0.03 mg/kg), and maintained with continuous intravenous infusions of fentanyl citrate (0.1 mg/kg/h), midazolam (1.5 mg/kg/h), and inhaled isoflurane (1–5% in oxygen). A bronchoscope was placed in the lower lobe of a single lung, and gastric contents (2 g/kg) were delivered as the tip of the bronchoscope was withdrawn to approximately 1 cm distal to the carina. After delivery, gastric contents were left to dwell for 6 h to induce severe acute lung injury *in vivo*.

Swine lungs with gastric aspiration injury were procured as previously described.[5,6,8] Swine lung donors were maintained under general anesthesia. Before skin incision, cefazolin (30 mg/kg) was administered intravenously. At the time of procurement, a median sternotomy was performed. A bolus of heparin (30,000 IU) was administered intravenously, and a cannula (16 Fr, Medtronic) was secured in the main pulmonary artery. Blood was drawn, collected in citrate–phosphate–dextrose collection bags (Chinook Medical), and stored at 8°C until the cross-circulation circuit was primed. When a non-perfusing rhythm was observed, a cold anterograde flush with 1 L low-potassium dextran organ preservation solution (Perfadex, XVIVO) with alprostadil (25 mg/kg) at 4°C was performed, and the left atrial appendage and superior vena cava were transected. Lungs were topically cooled with wet laparotomy sponges at 4°C, inflated to an airway pressure of 15 cmH_2O, and stapled across the trachea using a surgical stapler (TA, Covidien). The heart and lungs were explanted *en bloc* and placed on a sterile ice slurry at 4°C on a sterile back table. The heart was removed, and a left atrial cuff height of 5 mm was retained. A retrograde flush with 1 L organ preservation solution at 4°C was performed. The aortic arch was dissected, and the brachiocephalic and left subclavian branches were ligated or stapled. A 4-cm section of aorta was retained on both sides of these vessels to facilitate anastomosis to the left atrial cuff at one end and placement of the pulmonary vein cannula through the other end. After explant, swine lungs with gastric aspiration injury were placed in a sterile isolation bag with 500 mL organ preservation solution, maintained on a sterile ice slurry at 4°C, cannulated, placed on cross-circulation, and used to develop diagnostic and therapeutic modalities.

Ischemia–reperfusion injury

A swine model of ischemia–reperfusion injury was used to induce a severe acute lung injury that often renders donor lungs unacceptable for transplantation. Miniature swine from a herd of partially inbred swine with well-defined major histocompatibility complex loci were used.[56] Swine lungs (n = 3) were procured from male swine age 5–7 months, with a median weight of 44 kg (range: 38–70 kg).

Swine lungs were procured as previously described.[8] Swine were sedated, anesthetized via intramuscular induction with Telazol (5 mg/kg) and buprenorphine hydrochloride (0.03 mg/kg), and maintained with continuous intravenous infusions of fentanyl citrate (0.1 mg/kg/h), midazolam (1.5 mg/kg/h), and inhaled isoflurane (1–5% in oxygen). Before skin incision, cefazolin (30 mg/kg) was administered intravenously. At the time of procurement, a median sternotomy was performed. A bolus of heparin (30,000 IU) was

administered intravenously, and a cannula (16 Fr, Medtronic) was secured in the main pulmonary artery. Blood was drawn, collected in citrate–phosphate–dextrose collection bags (Chinook Medical), and stored at 8°C until the cross-circulation circuit was primed. When a non-perfusing rhythm was observed, a cold anterograde flush with 1 L low-potassium dextran organ preservation solution (Perfadex, XVIVO) with alprostadil (25 mg/kg) at 4°C was performed, and the left atrial appendage and superior vena cava were transected. Lungs were topically cooled with wet laparotomy sponges at 4°C, inflated to an airway pressure of 15 cmH_2O, and stapled across the trachea using a surgical stapler (TA, Covidien). The heart and lungs were explanted *en bloc* and placed on a sterile ice slurry at 4°C on a sterile back table. The heart was removed, and a left atrial cuff height of 5 mm was retained. A retrograde flush with 1 L organ preservation solution at 4°C was performed. The aortic arch was dissected free, and the brachiocephalic and left subclavian branches were ligated or stapled. A 4-cm section of aorta was retained on both sides of these vessels to facilitate anastomosis to the left atrial cuff at one end and placement of the pulmonary vein cannula through the other end.

After explant, lung ischemia–reperfusion injury was induced as previously described.[8] Swine lungs were placed in a sterile isolation bag with 500 mL organ preservation solution, and stored on ice at 4°C. After 18 h of static cold ischemia, swine lungs were cannulated and reperfused upon initiation of cross-circulation to induce severe ischemia–reperfusion injury and used to develop diagnostic and therapeutic modalities.

Primary cells

Mesenchymal stromal cells

Human primary adipose-derived mesenchymal stromal cells (Lonza) isolated from lipoaspirates obtained from a normal non-diabetic adult female donor during an elective surgical procedure were recovered from cryopreservation according to the manufacturer's instructions. Mesenchymal stromal cells were cultured *in vitro* according to the manufacturer's instructions in Dulbecco's modified Eagle's medium (DMEM) with high glucose supplemented with fetal bovine serum (10% v/v), penicillin/streptomycin (1% v/v), and basic fibroblast growth factor (0.1 ng/mL) at 100% humidity, 5% CO_2, and 37°C. Mesenchymal stromal cells were passaged at 70% confluency to prevent overgrowth and maintain stem cell characteristics and proliferative capacity, then used at passage 5 to develop delivery and tracking modalities.

Cell lines

Lung organoids

Human lung organoids were generated as previously described.[32,49] Human pluripotent stem cells (RUES2, passage 17–28) were cultured *in vitro* on a feeder layer of mouse embryonic fibroblasts plated at 15,000–18,000 cells/cm^2 in human pluripotent stem cell maintenance media at 100% humidity, 5% CO_2, and 37°C. To deplete mouse embryonic fibroblasts, human pluripotent stem cells were treated with Accutase (ThermoFisher Scientific) for 2 min at 37°C, added to 10-cm tissue culture dishes coated with basement membrane extract (Matrigel, Corning), and maintained for 24 h. To form embryoid bodies, human pluripotent stem cells were treated with trypsin (0.05% v/v, ThermoFisher Scientific) for 1 min at 37°C, and small clusters of human pluripotent stem cells were resuspended in serum-free differentiation media consisting of Dulbecco's modified Eagle's medium (DMEM)/Ham's F-12 (3:1 v/v, Life Technologies) supplemented with L-ascorbic acid (50 μg/mL, MilliporeSigma), B-27 Supplement (Gibco), bovine serum albumin (0.05% v/v, Life Technologies), GlutaMAX Supplement (2 mM, Life Technologies), monothioglycerol (0.4 μM, MilliporeSigma), *N*-2 Supplement (Life Technologies), and penicillin/streptomycin (1% v/v, ThermoFisher Scientific). Small clusters of human pluripotent stem cells were added to low-attachment 6-well plates (Corning) at a concentration of 10 clusters/well. Primitive streak formation was performed in serum-free differentiation media with addition of human bone morphogenic protein 4 (3 ng/mL, R&D Systems) and ROCK inhibitor Y-27632 (10 μM, Tocris) for 24 h. After primitive streak formation, endoderm induction was performed in serum-free differentiation media with addition of human activin A (100 ng/mL, R&D Systems), human basic fibroblast growth factor (2.5 ng/mL, R&D Systems), human bone morphogenic protein 4 (0.5 ng/mL, R&D Systems), and ROCK inhibitor Y-27632 (10 μM, Tocris) for 96 h. Half of the media volume was replaced every 48 h. On day 5, anterior foregut endoderm induction was performed. Embryoid bodies were treated with trypsin/EDTA (0.05% v/v, ThermoFisher Scientific) for 3 min at 37°C. Single cells were resuspended in serum-free differentiation media with addition of dorsomorphin dihydrochloride (1.5 μM, Tocris) and ALK4/5/7 inhibitor SB 431542 (10 μM, Tocris), added to 48-well plates (Corning) coated with fibronectin (MilliporeSigma) at a concentration of 70,000–100,000 cells/well, and maintained for 24 h. Media was replaced with serum-free differentiation media with addition of WNT signaling inhibitor IWP2 (1 μM, Tocris) and ALK4/5/7 inhibitor SB 431542 (10 μM, MilliporeSigma) for 24 h. On day 6–15, anterior foregut endoderm ventralization (branching) induction was performed in serum-free differentiation media with addition of all-trans retinoic acid (0–1 μM, MilliporeSigma), human bone morphogenic protein 4 (10 ng/mL, R&D Systems), human fibroblast growth factor 7 (10 ng/mL, R&D Systems), human fibroblast growth factor 10 (10 ng/mL, R&D Systems), murine epidermal growth factor (20 ng/mL, R&D Systems), and WNT signaling agonist CHIR99021 (3μM, Tocris) for 8–10 days. To induce airway epithelial cell maturation, on day 15–16, lung progenitor cells were treated with trypsin/EDTA (0.05% v/v, ThermoFisher Scientific) for 1 min at 37°C, and added to 48-well plates coated with fibronectin in serum-free differentiation media with addition of all-trans retinoic acid (50 nM, MilliporeSigma), human bone morphogenic protein 4 (10 ng/mL, R&D Systems), human fibroblast growth factor 7 (10 ng/mL, R&D Systems), human fibroblast growth factor 10 (10 ng/mL, R&D Systems), and WNT signaling agonist CHIR99021 (3μM, Tocris), and maintained until use. A detailed, step-by-step protocol describing the generation of lung organoids is available at *Nature Protocol Exchange*.[61] Lung organoids were used on day 17–22 to develop delivery and tracking modalities.

Please cite this article in press as: Pinezich et al., Theranostic methodology for *ex vivo* donor lung rehabilitation, Med (2025), https://doi.org/10.1016/j.medj.2025.100644

HEK-293FT cells

HEK-293FT cells (293FT, ThermoFisher Scientific), a fast-growing, highly transfectable clonal isolate derived from human embryonic kidney cells transformed with the SV40 large T antigen, were recovered from cryopreservation according to the manufacturer's instructions. HEK-293FT cells were cultured *in vitro* according to the manufacturer's instructions in Dulbecco's modified Eagle's medium (DMEM) with high glucose supplemented with heat-inactivated fetal bovine serum (10% v/v), L-glutamine (2 mM, MilliporeSigma), HEPES (2 mM, ThermoFisher Scientific), and penicillin/streptomycin (1% v/v) at 100% humidity, 5% CO_2, and 37°C. HEK-293FT cells were used to produce lentiviral particles containing the *Renilla reniformis* luciferase gene as previously described.[57,58] HEK-293FT cells were treated with trypsin/EDTA (0.05% v/v, ThermoFisher Scientific) for 2 min at 37°C, and added to 10-cm^2 tissue culture plates coated with poly-D-lysine (MilliporeSigma) at a concentration of 3 x 10^6 cells/plate. Lentiviral transfer vector DNA (PLox-hOCp:PLuc:GFP, PLox-hPECAM-1p:PLuc:GFP, PLox-HRE-12p:PLuc:GFP, CMV:hRLuc:RFP:ttk, 15 μg) was mixed with viral envelope plasmid (pMD-G-VSV-G, 5 μg), packaging construct (pCMV DR8.2, 10 μg), 450 μL water, and 50 μL calcium chloride (2.5 M, Sigma). Transfection solution was added dropwise to 500 μL HEPES at pH 7. Buffered transfection solution was incubated for 20 min at 25°C, added dropwise to HEK-293FT cells, and incubated for 24 h at 37°C. Transfection supernatant was removed, and HEK-293FT cells were rinsed with phosphate-buffered saline and incubated in serum-free media for 48 h. Supernatant containing lentiviral particles was collected, centrifuged at 400 xg, passed through a 0.45-μm low-protein-binding filter (Corning), loaded into an ultracentrifuge (L-100XP, Beckman Coulter), and ultracentrifuged at 26,000 rpm for 90 min at 4°C. Lentivirus particles were re-suspended in phosphate-buffered saline and stored at −80°C. Lentiviral titers were determined by enzyme-linked immunosorbent assay (HIV-1 p24 Antigen ELISA Kit, Beckman Coulter). Lentiviral particles were used to transduce human mesenchymal stromal cells with the *Renilla reniformis* luciferase gene, resulting in bioluminescent mesenchymal stromal cells that were used to develop delivery and tracking modalities.

METHOD DETAILS

As the depth of diagnostic assessment and extent of therapeutic intervention required for *ex vivo* lung rehabilitation is inherently variable across donor lungs, in cases where specific assessments and interventions are not predefined, we use the designation 'as needed' to indicate that the *ex vivo* lung rehabilitation team should apply their clinical judgment based on a combination of clinical experience and knowledge, the quality and functional trajectory of the *ex vivo* lungs, and close coordination with the transplant team to ensure that decisions align with the information needed to optimize transplant outcomes.

Ex vivo lung support

Cross-circulation

Cross-circulation between *ex vivo* lungs and a support swine was performed as previously described.[5–9,60,62] The circuit was configured with the following components: pump console (Maquet), centrifugal pump (Maquet), reservoir (Maquet), and 3/8-inch medical tubing (Saint-Gobain). Before the procedure, circuit components were sterilized by ethylene oxide. Pressure transducers (Edwards Lifesciences), flow probes (Sonotec), and blood sampling ports (Medline) were integrated into the circuit at the pulmonary artery and pulmonary vein of *ex vivo* lungs. The circuit was primed with 1 L warm balanced crystalloid solution for xenogeneic cross-circulation, or with 1 L swine lung donor blood for allogeneic cross-circulation.

Support swine (n = 23; 3 female, 20 male) age 5–7 months, with a median weight of 73 kg (range: 55–123 kg) were fasted for 4 h, sedated, anesthetized via intramuscular induction with Telazol (5 mg/kg) and buprenorphine hydrochloride (0.03 mg/kg), and maintained with continuous intravenous infusions of fentanyl citrate (0.1 mg/kg/h), midazolam (1.5 mg/kg/h), and inhaled isoflurane (1–5% in oxygen). Support swine were intubated and maintained on continuous mandatory ventilation throughout cross-circulation. Before skin incision, cefazolin (30 mg/kg) was administered intravenously and re-dosed every 8 h. An auricular arterial catheter was placed for hemodynamic monitoring and blood sampling, while auricular venous and femoral central venous catheters were placed for drug administration. A urinary catheter was placed via open cystostomy for continuous bladder drainage.

Enrofloxacin (5 mg/kg) and cephalexin (25 mg/kg) were administered to support swine. Immunosuppression drugs were administered for xenogeneic and allogeneic cross-circulation. For support swine undergoing xenogeneic cross-circulation with human donor lungs, diphenhydramine (50 mg), methylprednisolone (1 g), and cobra venom factor (1 mg) were administered 4 h before initiation of cross-circulation. Tacrolimus (5 mg), methylprednisolone (125 mg), and mycophenolate (500 mg) were administered immediately before initiation of cross-circulation with human donor lungs. Methylprednisolone was re-dosed every 8 h while tacrolimus and mycophenolate were re-dosed every 12 h during cross-circulation with human donor lungs. For support swine undergoing allogeneic cross-circulation with swine lungs, methylprednisolone (1 g) was administered immediately before initiation of cross-circulation.

Bilateral internal jugular vein access was obtained using ultrasound guidance or open surgical cutdown. A bolus of heparin (30,000 IU for xenogeneic cross-circulation; 15,000 IU for allogeneic cross-circulation) was administered intravenously. Cannulas (15–21 Fr, Medtronic) were placed in each internal jugular vein using Seldinger technique and serial dilation. Cannulas were secured to the skin, and cervical incisions were closed. A continuous rate infusion of heparin (3,000 IU/h) was titrated using a whole blood microcoagulation system (HemoChron, Accriva Diagnostics) to maintain activated clotting time of 180–250 s throughout cross-circulation.

Ex vivo lungs were retrieved from cold storage, maintained on a sterile ice slurry at 4°C, cannulated via the pulmonary artery and pulmonary vein, and flushed with 1 L balanced crystalloid solution at 4°C to remove air from the vascular compartment. The trachea was intubated with an endotracheal tube (Medline).

Immediately before initiation of cross-circulation, calcium chloride (1 g) was administered to support swine. To initiate cross-circulation, *ex vivo* lungs and support swine were connected to the circuit using sterile wet-to-wet connection technique. Support swine vitals and hemodynamic parameters were continuously monitored and recorded throughout cross-circulation.

Lung-protective perfusion and ventilation of *ex vivo* lungs were used throughout cross-circulation procedures, as previously described.[9] Pressures, flows, and temperature were continuously monitored and recorded throughout cross-circulation procedures. *Ex vivo* lungs maintained on cross-circulation were used to develop diagnostic and therapeutic modalities.

Isolated ex vivo lung perfusion

Isolated *ex vivo* lung perfusion (EVLP) of swine lungs or human donor lungs that were declined for transplantation and consented for research use was performed in two scenarios: (*i*) during or after cross-circulation by temporarily disconnecting support swine from the circuit and conducting isolated EVLP for approximately 10 min, (*ii*) in the absence of cross-circulation by conducting isolated EVLP for approximately 6 h as previously described.[5,8,63] For isolated EVLP during or after cross-circulation, support swine were temporarily disconnected from the circuit using sterile tubing clamps. For isolated EVLP in the absence of cross-circulation, lungs were placed in an organ preservation chamber (XVIVO) maintained at 37°C and humidified with warm sterile water. Cannulae were secured in the pulmonary artery and pulmonary vein, and the circuit was primed with whole blood collected during lung procurement. Lungs were connected to the circuit, and flow was initially set to 5–10% of estimated cardiac output, with target pulmonary artery pressure of <15 mmHg and pulmonary vein pressure of 3–5 mmHg. The ventilator (Oxylog 3000 plus, Dräger) was initially set to volume control mode; respiratory rate, 6–8 bpm; tidal volume, 6–8 mL/kg; positive end-expiratory pressure (PEEP), 5 cmH_2O; FiO_2, 40%, and ventilation was initiated within 10 min. Lung-protective perfusion and ventilation of *ex vivo* lungs were used throughout isolated EVLP procedures. Pressures, flows, and temperature were continuously monitored and recorded throughout isolated EVLP procedures. *Ex vivo* lungs maintained on isolated EVLP were used to develop diagnostic and therapeutic modalities.

Delivery strategies

Bronchoscopic delivery

Bronchoscopic delivery was performed for diagnostic and therapeutic modalities using a flexible video bronchoscope (aScope 3, Ambu), syringe (5 or 10 mL), and processing display unit (aView Advance, Ambu). Deliverables including saline, carrier media, drugs, cells, organoids, and/or other agents, were injected into the airways via the bronchoscope (outer diameter: 3.8 mm; channel inner diameter: 0.8 mm; field of view: 80°; tip flexion in each direction: 120 ± 10°). Before delivery, the deliverable was prepared (e.g., surfactant warmed to 25°C; mesenchymal stromal cells suspended in carrier media at delivery dose), and bronchoscopy images and videos were acquired as described in the Bronchoscopy section of STAR Methods. At the time of delivery, the bronchoscope was inserted through the endotracheal tube and into a segmental bronchus of *ex vivo* lungs. In some cases, bronchoscopic delivery was focused on a region of interest (e.g., surfactant replacement in an atelectatic lobe). Importantly, cell-based deliverables were injected at a controlled rate (1 mL/s) to minimize shear stress during delivery. Immediately after injection of cell-based deliverables, additional carrier media (2 mL) was injected to flush residual cells or organoids from the bronchoscope into the *ex vivo* lungs. After delivery, bronchoscopy images and videos were acquired, exported, and processed for analysis.

Intravascular delivery

Intravascular delivery was performed for diagnostic and therapeutic modalities using a Luer lock syringe, 3-way stopcock, and accessory tubing. Deliverables including drugs and contrast agents were injected into the circuit through a port at the main pulmonary artery cannula, as previously described.[7] At the time of delivery, the syringe and accessory tubing were carefully primed to prevent introduction of air bubbles into the circuit during intravascular delivery. After delivery, accessory tubing was flushed with normal saline (1 mL) to clear any residual blood or deliverable.

Nebulized delivery

Nebulized delivery was performed for diagnostic and therapeutic modalities using a closed-circuit vibrating mesh nebulizer (Aerogen Solo, Aerogen) and ventilator (Oxylog 3000 plus, Drager). Deliverables including drugs and other agents were added to the nebulizer cup and nebulized through the endotracheal tube into the airways of *ex vivo* lungs as previously described.[7] Nebulized delivery was usually completed within 10 min. After delivery, the nebulizer was disconnected from the ventilator tubing.

Transpleural delivery

Transpleural delivery was performed for diagnostic and therapeutic modalities using a sterile syringe, hypodermic needle (PrecisionGlide, BD), and sterile surgical marker (Medline). The delivery site was demarcated on the visceral pleura using a sterile surgical marker. Deliverables including diagnostic agents, cells, and organoids, were injected through the pleura using a sterile syringe (1, 5, or 10 mL) with a sterile hypodermic needle (27G x 1.25 in, 0.4 mm × 30 mm). At the time of delivery, an inspiratory hold was performed at peak inspiratory pressure to prevent the lungs from moving during transpleural delivery. The needle was primed and carefully inserted at the delivery site through the visceral pleura of *ex vivo* lungs. The deliverable was injected as the needle was slowly withdrawn until approximately 5 mm from the tip of the needle, resulting in a localized distribution throughout the parenchyma of *ex vivo* lungs. After delivery, the needle was carefully withdrawn from *ex vivo* lungs, and gentle manual pressure was immediately applied over the injection site to prevent any backflow, air leak, or bleeding. Positive pressure mechanical ventilation was resumed,

Please cite this article in press as: Pinezich et al., Theranostic methodology for *ex vivo* donor lung rehabilitation, Med (2025), https://doi.org/10.1016/j.medj.2025.100644

and gentle manual pressure was maintained on the injection site for 1 min. In the event of air leak or bleeding, a collagen dressing (1 x 1 in, McKesson) was placed over the injection site. In some cases, transpleural delivery was performed at multiple time points and at multiple sites across *ex vivo* lungs.

Diagnostic modalities

Surface temperature imaging

Lung surface temperature imaging was performed using an infrared camera (T530, FLIR) and software (ResearchIR, FLIR). Before each procedure, the infrared camera was calibrated according to the manufacturer's instructions, secured 120 cm above the organ basin using a fixed mount, positioned and angled relative to the *ex vivo* lungs, and focused to ensure longitudinal consistency of surface temperature imaging throughout the procedure. Surface temperature imaging was performed at regular time points and as needed throughout each procedure. To standardize image acquisition, surface temperature images were acquired during a 5-s inspiratory hold at peak inspiratory pressure, a standard reference point in the respiratory cycle. In some cases, infrared camera zoom was adjusted to acquire surface temperature images of a region of interest (e.g., consolidated lobe). Lung surface temperature images were exported and processed for diagnostic analysis.

Lung weight

Lung weight assessments were performed using a digital scale (W-4830, WeighMax). Before each procedure, the scale was calibrated according to the manufacturer's instructions, placed inside the organ chamber under the organ basin, and tared to ensure longitudinal consistency of lung weight assessments throughout the procedure. Lung weight assessments were performed at baseline (i.e., immediately after explant), at regular time points during cross-circulation, and as needed throughout each procedure. At the time of assessment, excess blood or fluid in the organ basin was aspirated to ensure longitudinal consistency of lung weight assessments, and the scale was tared to ensure precision to 2 significant digits. Lung tissue samples collected for analysis were weighed to account for lung weight loss due to tissue sampling. To normalize lung weight assessments across procedures involving single and double lungs with differences in size and condition (e.g., edema, hemorrhage), lung weight assessments were reported as a percentage of baseline lung weight and plotted as a function of time for diagnostic analysis.

Global perfusion imaging

Global perfusion imaging was performed using a mobile X-ray unit (PXP-16HF, United Radiology Systems), contrast agent (iohexol), and software (DICOM Viewer, MicroDicom). At the time of assessment, the X-ray unit was aligned with the base plate, secured 120 cm above the organ basin using either a fixed mount or mobile stand adjustable arm, and positioned and angled relative to the *ex vivo* lungs to ensure longitudinal consistency of global perfusion imaging throughout the procedure. X-ray unit settings were adjusted to 2.2 mAs and 90 kVp. Global perfusion imaging with and without contrast angiography was performed at regular time points and as needed throughout each procedure. To standardize image acquisition, global perfusion images were acquired during a 5-s inspiratory hold at peak inspiratory pressure, a standard reference point in the respiratory cycle. For global perfusion imaging with contrast angiography, iohexol (20 mL) was administered into the pulmonary artery of *ex vivo* lungs, and global perfusion images were acquired after 10 s. Global perfusion images were exported and processed for diagnostic analysis.

Regional perfusion imaging

Regional perfusion imaging was performed using a laser speckle contrast imaging system (RFLSI-ZW, RWD Life Sciences) and software (RFLSI Analytical Software, RWD Life Sciences). Before each procedure, the laser speckle contrast imaging system was calibrated according to the manufacturer's instructions. At the time of assessment, the laser speckle contrast imaging system was secured 20 cm above the region of interest of *ex vivo* lungs, positioned and angled relative to the *ex vivo* lungs, and focused to ensure longitudinal consistency of regional perfusion imaging throughout the procedure. Laser speckle contrast imaging was performed at regular time points and as needed throughout each procedure. To standardize image acquisition, laser speckle contrast images were acquired during a 5-s inspiratory hold at peak inspiratory pressure, a standard reference point in the respiratory cycle. Laser speckle contrast images and videos were exported and processed for diagnostic analysis. Perfusion values measured in perfusion units per cm^2 were averaged over 20 s and reported as mean ± standard deviation for diagnostic analysis.

Bronchoscopy

Bronchoscopy was performed using a flexible video bronchoscope (aScope 3, Ambu) and processing display unit (aView Advance, Ambu) at regular time points and as needed throughout each procedure. The decision for bronchoscopic assessment and intervention was guided by clinical observations, including evidence of airway edema, secretions, atelectasis, and/or consolidation, identified through visual inspection, radiographic imaging, and/or blood gas analysis. Regular calibration of the bronchoscope and maintenance of sterility ensured consistent performance and reduced risk of contamination during procedures. At the time of bronchoscopic assessment, the bronchoscope (outer diameter: 3.8 mm; channel inner diameter: 0.8 mm; field of view: 80°; tip flexion in each direction: 120 ± 10°) was inserted through the endotracheal tube into a segmental bronchus of each lobe of *ex vivo* lungs. In some cases, bronchoscopy was focused on a region of interest (e.g., consolidated lobe), and targeted bronchoscopy was performed to enable localized diagnostic assessment and therapeutic intervention. In cases requiring therapeutic intervention, airway clearance was achieved via bronchoscope-assisted suctioning of secretions and debris. Bronchoscopy images and videos were acquired, exported, and processed for diagnostic analysis.

Bronchoresponse

Bronchoresponse assessments were performed using a closed-circuit vibrating mesh nebulizer (Aerogen Solo, Aerogen), bronchoconstrictor agent (methacholine), and ventilator (Oxylog 3000 plus, Drager). Bronchoresponse assessments were performed as needed throughout each procedure. At the time of assessment, peak inspiratory pressure was continuously recorded using a ventilator for at least 1 min before administration of methacholine to establish a range of baseline values. Methacholine (100 mg/kg), a nonselective muscarinic receptor agonist that acts on airway smooth muscle cell membrane-bound receptors to induce bronchoconstriction, was nebulized and delivered to *ex vivo* lungs. Peak inspiratory pressure was continuously recorded using a ventilator during and for at least 1 min after nebulized delivery of methacholine or until a stable range of response values was established. Peak inspiratory pressure values were reported as a function of time for diagnostic analysis.

Airway cilia motility

Airway cilia motility assessments were performed using an airway tissue biopsy, glass bottom dish (MatTek), fluorescent polystyrene microspheres (FluoSpheres, Invitrogen), silicone supported coverglass (SecureSlip, Grace Bio-Labs), fluorescence microscope (IX 81, Olympus), high-speed front-illuminated CMOS camera (Zyla 5.5, Andor), and software (NIS Elements Advanced Research, Nikon). At the time of assessment, an airway tissue biopsy was collected, dissected into 2 mm^2 sections, placed lumen down onto a 50-mm glass bottom dish, and submerged in phosphate-buffered saline containing 0.2-μm fluorescent microspheres (1% v/v). A silicone supported coverglass was placed on the tissue biopsy to flatten the sample and exclude air bubbles, and excess solution was removed using a micropipette. The camera was focused on the inverted airway tissue biopsy, and airway cilia motility was assessed by video microscopy (100 frames/second). Bright-field video of airway cilia and fluorescence video of the movement of fluorescent microspheres due to airway cilia motility were acquired. Airway cilia motility videos were exported and processed for diagnostic analysis. Fluorescence images were extracted at two time points separated by a 3-s interval, and the movement of at least 6 fluorescent microspheres was tracked over at least 50 μm to assess airway cilia motility for diagnostic analysis.

Cytopathology (BAL fluid)

Cytopathology assessments were performed using a flexible video bronchoscope (aScope 3, Ambu), normal saline, specimen trap, periodic acid–Schiff staining, light microscope (FSX100, Olympus), and software (ImageJ, NIH). At the time of assessment, a bronchoscope (outer diameter: 3.8 mm; channel inner diameter: 0.8 mm; field of view: 80°; tip flexion in each direction: 120 ± 10°) was inserted into a segmental bronchus, and sterile normal saline (5 mL) was injected into the airway. After 5 s, bronchoalveolar lavage (BAL) fluid was aspirated into a sterile specimen trap. BAL fluid (100 μL) was smeared onto a glass slide, and air dried. BAL fluid smears were oxidized in periodic acid solution (0.5%) for 5 min, rinsed three times in deionized water for 1 min, placed in Schiff's reagent for 15 min, washed in tap water for 5 min, counterstained in Mayer's hematoxylin for 1 min, washed in tap water for 5 min, rinsed in deionized water for 1 min, dehydrated, mounted, coverslipped, and imaged under bright-field. Cytopathology images were exported and processed for diagnostic analysis. Cell counts were performed using the cell counter plugin of the image analysis software. Cell counts measured in cells per high-power field (hpf) were averaged over 5 high-power fields and reported as mean ± standard deviation for diagnostic analysis.

Total protein (BAL fluid)

Total protein assessments of BAL fluid were performed using a flexible video bronchoscope (aScope 3, Ambu), normal saline, specimen trap, 96-well plate (ThermoFisher Scientific), protein assay (Pierce Coomassie Bradford Protein Assay Kit, ThermoFisher Scientific), and microplate reader (Synergy H1, BioTek). At the time of assessment, a bronchoscope (outer diameter: 3.8 mm; channel inner diameter: 0.8 mm; field of view: 80°; tip flexion in each direction: 120 ± 10°) was inserted into a segmental bronchus, and sterile normal saline (5 mL) was injected into the airway. After 5 s, bronchoalveolar lavage (BAL) fluid was aspirated into a sterile specimen trap. BAL fluid was centrifuged at 3,500 rpm for 10 min at 4°C. BAL fluid samples (5 μL) and bovine serum albumin standards (5 μL) were added to a 96-well plate in triplicate. Bradford reagent (250 μL) was added to each well. The 96-well plate was shaken for 30 s, incubated for 10 min at 25°C, and loaded into a microplate reader. Absorbance was measured at 595 nm. The average absorbance value of blank replicates was subtracted from the average absorbance values of BAL fluid samples and bovine serum albumin standards. A standard curve was generated by plotting the average blank-corrected measurement for each standard against its concentration. The standard curve was used to determine total protein concentration in BAL fluid for diagnostic analysis.

Airway inflammation (BAL fluid)

Airway inflammation was quantified using a flexible video bronchoscope (aScope 3, Ambu), syringe, normal saline, specimen trap, enzyme-linked immunosorbent assay (ELISA) kits for inflammatory cytokines IL-1β (ESIL1B, ThermoFisher Scientific), IL-6 (ESIL6, ThermoFisher Scientific), IL-10 (KSC0101, ThermoFisher Scientific), TNF-α (KSC3012, ThermoFisher Scientific), and microplate reader (Synergy H1, BioTek). At the time of assessment, a bronchoscope (outer diameter: 3.8 mm; channel inner diameter: 0.8 mm; field of view: 80°; tip flexion in each direction: 120 ± 10°) was inserted into a segmental bronchus, and sterile normal saline (5 mL) was injected into the airway. After 10 s, bronchoalveolar lavage (BAL) fluid was aspirated into a sterile specimen trap. BAL fluid was centrifuged at 3,500 rpm for 10 min at 4°C. BAL fluid samples and inflammatory cytokine standards were added to ELISA plates in triplicate and analyzed according to the manufacturer's instructions. For each inflammatory cytokine, a standard curve was generated by plotting the average blank-corrected measurement for each standard against its concentration. Standard curves were used to determine inflammatory cytokine concentrations in BAL fluid for diagnostic analysis.

Please cite this article in press as: Pinezich et al., Theranostic methodology for *ex vivo* donor lung rehabilitation, Med (2025), https://doi.org/10.1016/j.medj.2025.100644

Oxygenation test

Oxygenation testing was performed using a syringe and point-of-care blood analysis system (Heska, Element POC). Oxygenation 'challenges' were performed at regular time points and as needed throughout each procedure. At the time of assessment, 'pre-challenge' blood (0.5 mL) was drawn from sampling ports at the pulmonary artery and pulmonary vein. In some cases, *ex vivo* lungs had predominantly unilateral injury (e.g., left-sided gastric aspiration), and single-lung pulmonary venous blood was drawn from cannulae placed separately in the left and right pulmonary veins. 'Pre-challenge' blood was loaded into the point-of-care blood analysis system, and pre-challenge pO_2 was recorded. After pre-challenge values were obtained, the fraction of inspired oxygen (FiO_2) was increased to 100%, and minute ventilation was increased by 100%. After 10 min, 'post-challenge' blood (0.5 mL) was drawn from sampling ports at the pulmonary artery and main/left/right pulmonary vein, loaded into the point-of-care blood analysis system, and post-challenge pO_2 was recorded. Changes in pO_2 were determined using the following equation:

$$\Delta pO_2 = pO_2(\text{post challenge}) - pO_2(\text{pre challenge})$$

After testing, the fraction of inspired oxygen (FiO_2) and minute ventilation were returned to pre-challenge settings. ΔpO_2 values were used for diagnostic analysis.

Ventilation test

Ventilation testing was performed using a syringe and point-of-care blood analysis system (Heska, Element POC). Ventilation 'challenges' were performed at regular time points and as needed throughout each procedure. At the time of assessment, 'pre-challenge' blood (0.5 mL) was drawn from sampling ports at the pulmonary artery and pulmonary vein. In some cases, *ex vivo* lungs had predominantly unilateral injury (e.g., left-sided gastric aspiration), and single-lung pulmonary venous blood was drawn from cannulae placed separately in the left and right pulmonary veins. 'Pre-challenge' blood was loaded into the point-of-care blood analysis system, and pre-challenge pCO_2 was recorded. After pre-challenge values were obtained, the fraction of inspired oxygen (FiO_2) was increased to 100%, and minute ventilation was increased by 100%. After 10 min, 'post-challenge' blood (0.5 mL) was drawn from sampling ports at the pulmonary artery and main/left/right pulmonary vein, loaded into the point-of-care blood analysis system, and post-challenge pCO_2 was recorded. Changes in pCO_2 were determined using the following equation:

$$\Delta pCO_2 = pCO_2(\text{post challege}) - pCO_2(\text{pre challenge})$$

After testing, the fraction of inspired oxygen (FiO_2) and minute ventilation were returned to pre-challenge settings. ΔpCO_2 values were used for diagnostic analysis.

Vasoresponse

Vasoresponse assessments were performed using a vasoconstrictor agent (phenylephrine) and pressure transducers (Edwards Lifesciences) at the pulmonary artery and pulmonary vein. Vasoresponse assessments were performed as needed throughout each procedure. At the time of assessment, *ex vivo* lungs on cross-circulation support were temporarily disconnected from support swine and maintained on isolated *ex vivo* lung perfusion to preclude effects of support swine. Circuit pressures at the pulmonary artery and pulmonary vein were continuously recorded using pressure transducers for at least 15 s before administration of phenylephrine to establish a range of baseline values. Phenylephrine (4 mg), a selective α_1-adrenergic receptor agonist that acts directly on vascular smooth muscle cell membrane-bound receptors to induce vasoconstriction, was injected into the pulmonary artery of *ex vivo* lungs. Circuit pressures at the pulmonary artery and pulmonary vein were continuously recorded using pressure transducers during and for at least 45 s after intravascular delivery of phenylephrine or until a stable range of response values was established. After assessment, *ex vivo* lungs were reconnected to support swine, and cross-circulation was resumed. Circuit pressure values at the pulmonary artery and pulmonary vein were reported as a function of time for diagnostic analysis.

Metabolic activity

Metabolic activity assessments were performed using a surgical stapler (EndoGIA, Medtronic), surgical scalpel, 96-well plate (ThermoScientific Pierce), metabolic activity assay (alamarBlue Cell Viability Reagent, ThermoFisher Scientific), and microplate reader (Synergy H1, BioTek). The metabolic activity assay reagent resazurin enters live cells and is reduced to the fluorescent red compound resorufin, enabling quantitative assessments of metabolic activity. Metabolic activity assessments were performed at baseline and as needed throughout each procedure. A parenchymal tissue biopsy (1 g) was collected using a surgical stapler, finely minced (1 mm^3) using a sterile scalpel, rinsed with sterile phosphate-buffered saline, patted dry with sterile tissue, and suspended in Dulbecco's modified Eagle's medium (DMEM) with high glucose supplemented with fetal bovine serum (10% v/v) and metabolic activity assay reagent (10% v/v). Parenchymal tissue samples (1 mm^3/well) and metabolic activity reagent (100 μL/well) were placed in a 96-well plate in triplicate. The 96-well plate was covered with aluminum foil and incubated at 37°C with gentle shaking for 120 min. Supernatant (100 μL/well) was transferred into a new 96-well plate, and absorbance was measured at 570 nm and 600 nm (reference wavelength). The average absorbance value of blank replicates (metabolic activity assay reagent only) was subtracted from the average absorbance values of parenchymal tissue samples. Triplicates were averaged to obtain metabolic activity values in arbitrary units for diagnostic analysis.

Cell viability

Cell viability assessments were performed using carboxyfluorescein succinimidyl ester (CFSE, Abcam), 4′,6-diamidino-2-phenylindole (DAPI, ThermoFisher Scientific), a surgical stapler (EndoGIA, Medtronic), formalin-free fixative (Accustain, Sigma-Aldrich), automated tissue processor (Tissue-Tek VIP 5, Sakura Finetek), and fluorescence microscope (FSX100, Olympus). The cell viability reagent carboxyfluorescein diacetate succinimidyl ester (CFDASE) enters live cells and is cleaved by intracellular esterases to generate carboxyfluorescein succinimidyl ester (CFSE), a fluorescent compound. CFSE reacts with intracellular free amines to generate covalent fluorescent compound–protein conjugates, resulting in intracellular fluorescent labeling of live cells that is retained after chemical fixation. Cell viability assessments were performed as needed throughout each procedure. At the time of assessment, cell viability reagent CFDASE (1.06 M) was prepared in dimethyl sulfoxide and delivered by transpleural injection (1 mL) into a region of interest (e.g., consolidated lobe). After 15 min, a parenchymal tissue biopsy (5 g) was collected using a surgical stapler, dissected using a surgical scalpel, rinsed in phosphate-buffered saline, and fixed in formalin-free fixative at 4°C for 1 h. Fixed tissue samples were dehydrated, cleared, embedded, and sectioned using an automated tissue processor. Sections were de-paraffinized, stained with DAPI to visualize cell nuclei, rinsed, mounted, and imaged using a fluorescence microscope. Cell viability images were exported and processed for diagnostic analysis.

Surfactant uptake

Surfactant uptake assessments were performed using a flexible video bronchoscope (aScope 3, Ambu), surfactant protein B tagged with a green fluorescent dye (BODIPY FL Succinimidyl Ester, Invitrogen), surgical stapler (EndoGIA, Medtronic), and two-photon confocal fluorescence microscope (TCS SP8, Leica). Surfactant protein B was tagged with fluorescent dye BODIPY to obtain BODIPY-SPB, as previously described.[7] Surfactant uptake assessments were performed as needed throughout each procedure. At the time of assessment, BODIPY-SPB (20 ng/mL) was delivered by transpleural injection (1 mL) into a region of interest (e.g., consolidated lobe). After 30 min, a parenchymal tissue biopsy (5 g) was collected using a surgical stapler, dissected using a surgical scalpel, rinsed in phosphate-buffered saline, and imaged using a two-photon confocal fluorescence microscope. Surfactant uptake images were exported and processed for diagnostic analysis.

Therapeutic modalities

Bronchoalveolar lavage

Bronchoalveolar lavage was performed using a flexible video bronchoscope (aScope3, Ambu), syringe, and sterile normal saline as needed throughout each procedure to clear gastric contents, secretions, and/or cellular debris from *ex vivo* lungs. A bronchoscope (outer diameter: 3.8 mm; channel inner diameter: 0.8 mm; field of view: 80°; tip flexion in each direction: 120 ± 10°) was inserted into a segmental bronchus of the *ex vivo* lung. Through the bronchoscope, sterile normal saline (10 mL) was injected. After 5 s, bronchoalveolar lavage (BAL) fluid was aspirated into a sterile specimen trap. Five-minute intervals were interspersed throughout the lavage procedure to prevent prolonged interruptions in *ex vivo* lung ventilation. The maximum volume of bronchoalveolar lavage fluid per intervention was 50 mL. The total volume of bronchoalveolar lavage fluid did not exceed 300 mL, consistent with previously described bronchoalveolar lavage strategies.[5]

Surfactant replacement

Surfactant replacement was performed using a flexible video bronchoscope (aScope3, Ambu), syringe, and pulmonary surfactant (bovine lipid extract surfactant, BLES Biochemicals) as needed throughout each procedure. Immediately after bronchoalveolar lavage, a bronchoscope (outer diameter: 3.8 mm; channel inner diameter: 0.8 mm; field of view: 80°; tip flexion in each direction: 120 ± 10°) was inserted into a segmental bronchus of the *ex vivo* lung. Pulmonary surfactant (3 mL) was warmed to 25°C immediately before use. At the time of use, pulmonary surfactant (27 mg phospholipids/mL) was delivered by bronchoscopic injection into *ex vivo* lungs. The total dose of pulmonary surfactant was 12.5 mg phospholipid/kg (lung donor body weight), consistent with previously described surfactant replacement strategies.[5]

Recruitment maneuvers

Recruitment maneuvers were performed by adjusting the settings of the mechanical ventilator and, if necessary, manually manipulating *ex vivo* lungs. Recruitment maneuvers were applied immediately after surfactant replacement and/or as needed throughout the procedure to transiently increase the airway positive pressure gradient, open collapsed alveoli, and increase vital capacity. Tidal volume was increased by 15–20%, positive end-expiratory pressure (PEEP) was increased up to 12.5 cmH_2O, and inspiratory holds were performed with peak airway pressures up to 25 cmH_2O. Recruitment maneuvers were performed for 10 min, and lung protective ventilator settings were restored. When possible, manual recruitment maneuvers were performed in a manner consistent with techniques used during clinical lung transplantation. During inspiration, gentle compression was applied manually to areas of aerated lung, thereby directing ventilation toward regions of atelectatic non-aerating lung and facilitating recruitment. To avoid barotrauma and the deleterious effects of hyperinflation, peak inspiratory pressure was maintained below 30 cmH_2O during all recruitment maneuvers. Total recruitment time per procedure did not exceed 60 min.

Please cite this article in press as: Pinezich et al., Theranostic methodology for *ex vivo* donor lung rehabilitation, Med (2025), https://doi.org/10.1016/j.medj.2025.100644

Cell-based deliverables

Delivery of mesenchymal stromal cells

Mesenchymal stromal cells were used to develop (*i*) bronchoscopic and transpleural delivery modalities and (*ii*) fluorescence and bioluminescence tracking techniques in *ex vivo* lungs with no injury. Mesenchymal stromal cells labeled with fluorescent carboxyfluorescein succinimidyl ester (CFSE, Abcam) were used to develop bronchoscopic delivery, and mesenchymal stromal cells transduced with bioluminescent luciferase were used to develop transpleural delivery. Delivery of fluorescent or bioluminescent mesenchymal stromal cells was performed as needed throughout each procedure. At the time of delivery, fluorescent mesenchymal stromal cells were counted and suspended in phosphate-buffered saline (carrier media) at a concentration of 30 x 10^6 cells/mL, and loaded into a sterile syringe. Bioluminescent mesenchymal stromal cells were counted and suspended in phosphate-buffered saline (carrier media) at a concentration of 1.0 x 10^5 cells/mL, 2.5 x 10^5 cells/mL, 5.0 x 10^5 cells/mL, or 1.0 x 10^6 cells/mL, and loaded into a sterile syringe. Technical descriptions of bronchoscopic and transpleural delivery are in the 'Delivery modalities' section.

Delivery of lung organoids

Lung organoids constitutively expressing fluorescent ZsGreen were used to develop transpleural delivery and fluorescence tracking of organoids in *ex vivo* lungs with no injury. Delivery of fluorescent lung organoids was performed as needed throughout each procedure. At the time of delivery, fluorescent lung organoids (1–2 x 10^7 cells) were suspended in branching media (0.5–3 mL) and loaded into a sterile syringe. Technical description of transpleural delivery is in the 'Delivery modalities' section.

Tracking techniques

Fluorescence tracking

Real-time, non-invasive, automated detection and quantification of fluorescent mesenchymal stromal cells delivered into *ex vivo* lungs during cross-circulation were performed using a custom transpleural fluorescence microscopy system and custom computer vision algorithm (Figure S4B). The target-tracking transpleural fluorescence microscopy system was comprised of the following optical components: target camera for macroscopic identification of target regions (Mako), acquisition camera for capture of microscopic images (Zyla 4.2, Andor), mercury lamp (Intensilight, Nikon), objective lenses (10×, 20x, UPlanFL, Olympus), and optical filters (Semrock). The acquisition camera was secured to a dynamic articulating mount controlled by servomotors (HITEC RCD USA) and a custom computer vision algorithm (MATLAB, Mathworks). Before each procedure, the target-tracking transpleural fluorescence microscopy system was calibrated. Bronchoscopic delivery was performed for fluorescent mesenchymal stromal cells, and transpleural delivery was performed for fluorescent lung organoids. At the time of tracking, during continuous positive-pressure ventilation, fluorescent cells delivered into *ex vivo* lungs were automatically detected and quantified in real time by an image analysis program in the custom computer vision algorithm, which identified and counted bright spots in each frame of a live video to generate a quantitative plot in real time. Real-time fluorescence tracking was used to inform the location, distribution, and status of cells delivered into *ex vivo* lungs during cross-circulation.

Fluorescence tracking of fluorescent cells and organoids delivered into *ex vivo* lungs was validated using a surgical stapler (EndoGIA, Medtronic), formalin-free fixative (Accustain, Sigma-Aldrich), automated tissue processor (Tissue-Tek VIP 5, Sakura Finetek), and fluorescence microscope (FSX100, Olympus). At 36 h of cross-circulation, 18 h after delivery of fluorescent cells, parenchymal tissue samples were collected using a surgical stapler, dissected using a surgical scalpel, rinsed in phosphate-buffered saline, and fixed in formalin-free fixative at 4°C for 1 h. Fixed tissue samples were dehydrated, cleared, embedded, and sectioned using an automated tissue processor. Sections were de-paraffinized, immunostained, rinsed, mounted, and imaged using a fluorescence microscope. Fluorescent immunohistochemical staining images were exported and processed for diagnostic analysis.

Bioluminescence tracking

Real-time, non-invasive detection and quantification of bioluminescent mesenchymal stromal cells delivered into *ex vivo* lungs during cross-circulation were performed using a custom transpleural bioluminescence microscopy system. The transpleural bioluminescence microscopy system was comprised of the following optical components: scientific CMOS camera (Zyla 4.2, Andor), objective lenses (10×, 20x, Plan N, Olympus), and light-tight black box (Figure S4B). Bioluminescent mesenchymal stromal cells were generated by stable transduction of *Renilla reniformis* luciferase using a lentiviral vector, as previously described.[57,58] The lentiviral vector construct used to transduce mesenchymal stromal cells contained a chimeric sequence (CMV:hRLuc:mRFP:ttk) for the *Renilla* luciferase reporter gene hRLuc and the monomeric red fluorescent protein gene mRFP1 under transcriptional control of the CMV promoter.[57,58] Human embryonic kidney HEK-293FT cells were transfected with lentiviral vector construct (32.73 μg CMV·hRLuc:mRFP:ttk), VSV-G envelope expressing plasmid (10.91 μg pMD2.G, Addgene), and HIV-1 GAG/POL, Tat, and Rev packaging plasmid (21.82 μg pCMV delta R8.2, Addgene) using polyethylenimine (Polysciences). After 60 h, HEK-293FT cell culture supernatant was passed through a 0.45-μm low protein-binding filter (Steriflip-HV, Millipore), and viral particles were precipitated using a lentivirus concentration reagent (Lenti-X Concentrator, Takara Bio). To transduce mesenchymal stromal cells, concentrated virus at a multiplicity of infection of 15 (2 × 10^6 TU/mL) and hexadimethrine bromide (8 μg/mL Polybrene, Sigma-Aldrich) were added to mesenchymal stromal cell media. After 48 h, viral transduction efficiency was determined by detection of red fluorescent protein (RFP) using fluorescence microscopy, and fluorescent cells were selected using fluorescence-activated cell sorting (FACS). Mesenchymal stromal cells expressing 10% fluorescence intensity were selected, expanded, and used at passage 5.

Transpleural delivery was performed for bioluminescent mesenchymal stromal cells. At the time of delivery, bioluminescent mesenchymal stromal cells were suspended in phosphate-buffered saline (at a concentration of 1 x 10^5, 2 x 10^5, 4 x 10^5, 8 x 10^5 cells;

0.5 mL/dose; 3–30 x 10^6 cells/mL), treated with *Renilla* luciferase substrate (Promega), and delivered within 15 min into a segment of *ex vivo* lungs. Technical description of transpleural delivery is in the 'Delivery modalities' section. At the time of tracking, bright-field images were acquired to contextualize bioluminescence signals. Five minutes after administration of *Renilla* luciferase substrate, a wedge biopsy of the delivery region was obtained and visualized using the bioluminescent imager with acquisition times of 1–30 s. To quantify the number of bioluminescent mesenchymal stem cells in a region of interest in *ex vivo* lungs, a standard multi-well plate with defined numbers of bioluminescent mesenchymal stem cells was used to generate a standard curve of luciferase activity (number of photons emitted by cells, measured in arbitrary units (au) as luminescence signal intensity) as a function of bioluminescent mesenchymal stem cell number based on the maximum cumulative signal strength of a region of interest as previously described.[57,58] Photon counts (PC) were quantified after background subtraction using the following equation:

$$PC = (\text{Total PC in ROI}) - [(\text{Pixels in ROI}) \times (\text{Average Background PC} / \text{Pixel})]$$

A color bar representing standard light intensity (blue: low; red: high) was used for all images acquired at a timepoint.

Bioluminescence tracking of delivered bioluminescent cells was validated using a surgical stapler (EndoGIA, Medtronic), formalin-free fixative (Accustain, Sigma-Aldrich), automated tissue processor (Tissue-Tek VIP 5, Sakura Finetek), and virtual slide microscope (BX61VS, Olympus). At 36 h of cross-circulation, 18 h after delivery of bioluminescent cells, parenchymal tissue samples were collected using a surgical stapler, dissected using a surgical scalpel, rinsed in phosphate-buffered saline, and fixed in formalin-free fixative at 4°C for 1 h. Fixed tissue samples were dehydrated, cleared, embedded, and sectioned using an automated tissue processor. Sections were de-paraffinized, immunostained with anti-RLuc antibody, rinsed, mounted, and imaged using a fluorescence microscope. Fluorescent immunohistochemical staining images were exported and processed for diagnostic analysis.

QUANTIFICATION AND STATISTICAL ANALYSIS

This study is based on $n = 23$ independent experiments, where n represents an individual cross-circulation procedure between a human donor lung and support swine, or between a swine donor lung and support swine. All samples were analyzed as technical replicates in triplicate. Representative results in the form of a longitudinal comparison between two timepoints (e.g., baseline versus endpoint) or from a single timepoint (e.g., midpoint, endpoint) from exemplary cases ($n = 1$) are reported for each modality. All graphs were prepared using statistical analysis software (Prism version 10, GraphPad).